The Thesis committee for Vishal Nayyar
Certifies that this is the approved version of the following thesis:

Stretch-Induced Compressive Stress and Wrinkling in Elastic Thin Sheets

APPROVED BY
SUPERVISING COMMITTEE:

Supervisor: ______________________________
Rui Huang

____
K. Ravi-Chandar

Stretch-Induced Compressive Stress and Wrinkling in Elastic Thin Sheets

by

Vishal Nayyar, B.E.

Thesis

Presented to the Faculty of the Graduate School

of the University of Texas at Austin

in Partial Fulfillment

of the Requirements

for the Degree of

Master of Science in Engineering

The University of Texas at Austin

August, 2010

Dedicated

To My

Parents

Acknowledgements

First and foremost I would like to thank my advisor, Dr. Rui Huang. He not only guided me through this research but always made sure that I received the kind of support that I needed along the way. Without his support, this work would not have been possible. I would like to thank Dr. K. Ravi-Chandar for being part of the committee of this thesis and his valuable advice and comments. Apart from this I would like to thank all other faculty members of the Engineering Mechanics department at the UT Austin.

I would also like to thank my undergraduate professors (Dr L.C. Singal, Dr. L.D. Garg, Dr. Manu Sharma, A.P. Singh, Harvinder Singh) for instilling in me both curiosity and motivation for the post-graduate studies.

I've also been fortunate to have a great group of friends at UT Austin. This includes my office mates (Rohan, Adrein, Sharavan, Seung, Josh, John, Aaron, Wei, Nickolas, Ben) and many other students and faculty at UT. Special thanks goes to my many other friends (Mohit, Gautam, Aashish, Navjit, Girish, Vijay, Ankush, Rabia, Shilpa, Samriti, Gunjot, Sumit, Gitesh, Saurabh, Ranjiv, Emily, Aviral, Jennifer). Not only are you the people I can discuss my research with and goof off with, but also you are confidants who I can discuss my troubles with and who stand by me through all the times.

Last but not the least I must thank my family. Without their unending support and love from childhood to now, I never would have made it through this process or any of the tough times in my life. Thank you.

Stretch-Induced Compressive Stress and

Wrinkling in Elastic Thin Sheets

By

Vishal Nayyar, M.S.E.

The University of Texas at Austin, 2010

SUPERVISOR: Rui Huang

A finite element analysis approach is used to determine the susceptibility to wrinkles for thin sheets with clamped ends when subjected to tensile loading. The model problem chosen to do this analysis is the stretching of a thin sheet with clamped-ends. In the preliminary analysis, a stress analysis of thin sheets is done to study the stresses that develop under these boundary conditions. The analysis shows that there is a stretch-induced compressive stress in the transverse direction to the applied load that causes wrinkles. Then, the parametric study is conducted to determine the effect of aspect ratio and strain on the compressive stress. Based on the results of the parametric study, a critical strain value for each aspect ratio is determined for which the corresponding compressive stress is zero. Further buckling analysis is performed to find the buckling modes of the model problem that shows a limit of aspect ratio below which buckling is not possible under given conditions. Finally, post-buckling analysis shows the nature of wrinkles observed in the model problem for different aspect ratios.

Table of Contents

List of Tables

List of Figures

1. Introduction to thin sheet structures

1.1 Introduction

Thin sheet structures are being widely used in number of applications [1-5]. In recent years, thin sheet structures made of materials like Kapton has replaced traditional structures due to their light weight and low space requirement as compared to traditional structures. These structures can be in many shapes and sizes. For an effective structure, the surface flatness of the sheet is one of the key components for some applications while in others it can tolerate some wrinkles with a known small deviation from the nominal shape. The wrinkles in the sheets can be permanent or temporary. In this thesis we will analyze temporary wrinkles, which form as a result of loading. These types of wrinkles are called structural wrinkles. They form in regions of elastic buckling caused by the in-plane stresses in the sheet. The wrinkle behavior depends on the applied loads and boundary conditions. Such wrinkles can be removed and are therefore of great interest since it is possible to eliminate them through careful analysis and structural design. The constitutive behavior in such cases is difficult to predict because of the extreme nonlinearities that wrinkles can cause. Thus we are using a numerical approach to analyze these wrinkles. Following are few of the applications of thin sheet structures in which wrinkles can cause problems.

1.2 Applications

a) Space based solar radars

The *Synthetic Aperture Radar* (SAR) as shown in figure 1-1 is one of the technique that replaces the traditional radar. This technique uses both phase and amplitude of the signal received whereas the conventional radar only uses the amplitude, thus it allows high-resolution images. A larger SAR gives a better performance and hence it is required to produce large SAR and pack it into a space as small as possible. When it is required to inflate the packed SAR, it uses a planar frame to support and stretch the attached sheet. Hence in doing so, it may result in wrinkle formation in the sheet.

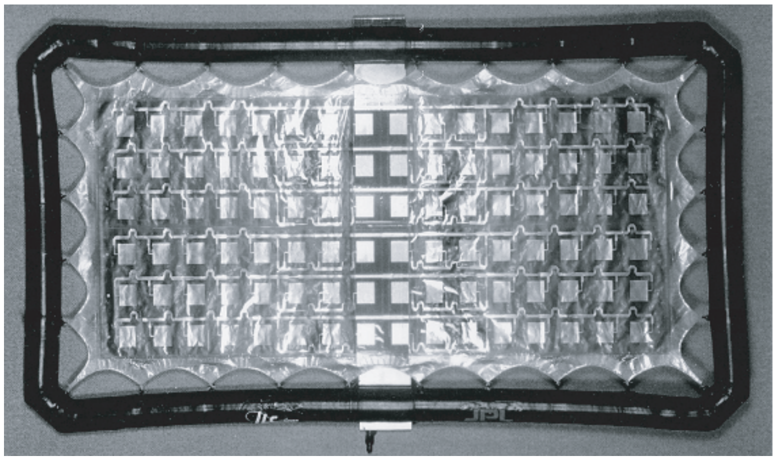

Figure 1-1: Synthetic Aperture Radar with an inflatable ring structure (from [6]).

b) Inflatable Antenna

A reflect array antenna as shown in figure 1-2 is based on the concept of a reflector sheet that is stretched flat by an attached inflatable frame.

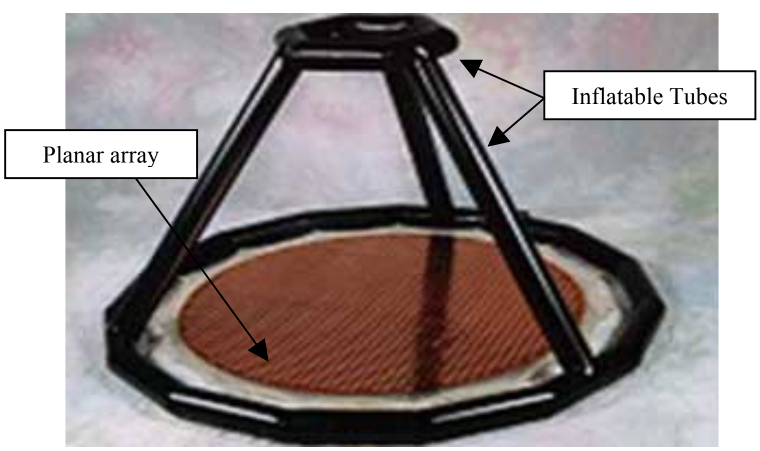

Figure 1-2: A space deployable inflatable antenna (from [7]).

The reflecting array in an antenna of this type is the planar array of micro strip patches printed on the thin circular sheet. An inflatable circular toroidal tube (frame) is attached to the edge of the sheet; when inflated, the tube stretches the circular sheet flat and supports the membrane in the operational configuration. A thin flexible material is folded prior to launch and then deployed by inflation.

c) Solar Sails

Solar sails work on the same concept as used in ships to move them. Just as ships uses sheet of cloth to catch wind for their movement, solar sails are made of thin polymer sheets coated with aluminum as shown in figure 1-3, provides the forward movement because of the hitting photons.

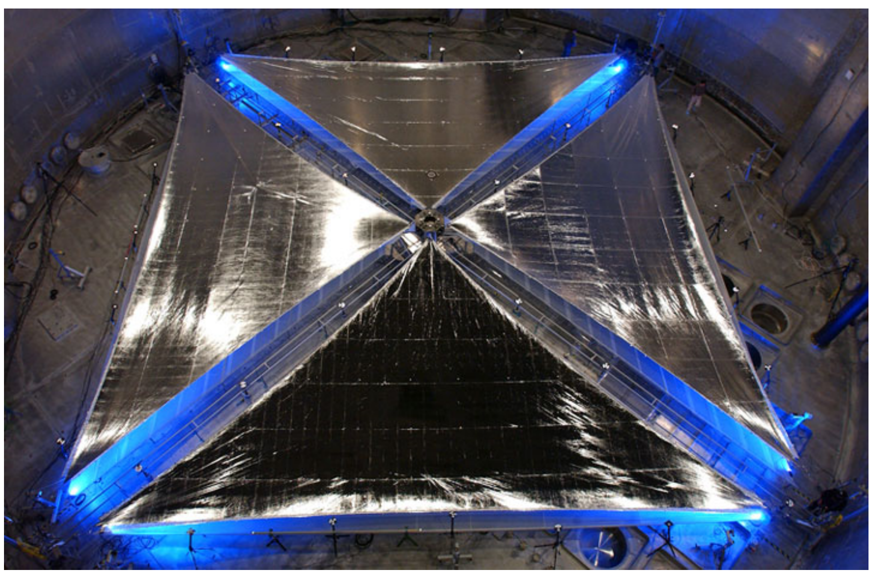

Figure 1-3: Solar sail (from [8]).

Photons exert force on everything they hit. This force is insignificant on earth because of earth's atmosphere. But in vacuum of space, photon pressure can actually move objects. When a solar sail is exposed to photon pressure, it will start to move. The forward motion is quite slow at first but with the unlimited fuel supply (sunlight) and under constant acceleration, the sail can move as fast as 3500 km/h in just a few months. For such an application, wrinkles can lead to problems such as non-concurrent centers of pressure and mass, reduced reflectivity, and non-uniform surface heating.

Other applications include future solar power arrays, space solar power shows great promise for future sources of energy and with thin-sheet arrays it is possible to have much higher specific power and larger arrays as compared to the current rigid solar arrays.

1.3 Model problem

After discussion of the applications of the thin sheets we can get an idea that wrinkling in thin sheets is one of the issues that we need to solve for their effective use. There have been various studies done on wrinkle formation, in which the wrinkles form either from shear, tension, or torsion [9-12]. In this thesis, we will concentrate on a model problem where wrinkles form due to tensile loading. Figure 1-4 shows an experimental observation of a sheet with aspect ratio, $L_o/W_o = 2.5$, stretched to 10% strain with the clamped-ends.

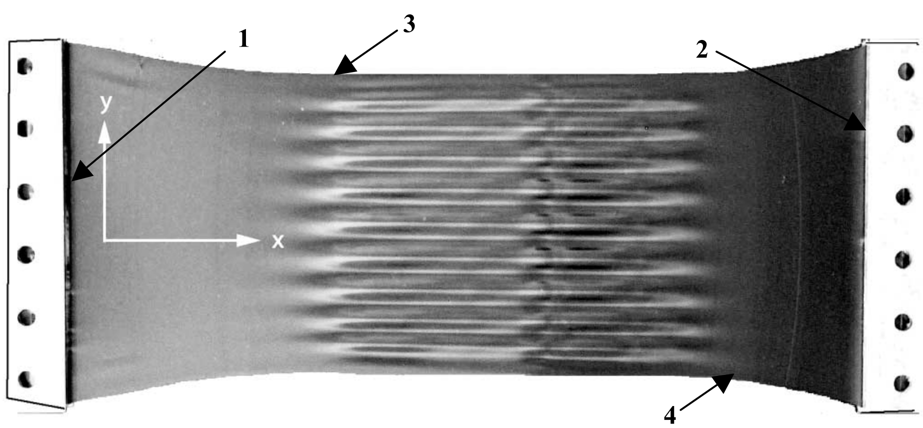

Figure 1-4: Wrinkles in a polyethylene sheet of length, L_o = 25cm, width, W_o = 10cm, and thickness, t_o = 0.01cm under a uniaxial tensile strain, ε_1 = 0.10 (from [13]).

Two ends of the sheet are clamped (ends 1 & 2 as marked in figure 1-4), so that they do not contract when the sheet is stretched along x-direction whereas the horizontal edges are free (ends 3 & 4 as marked in figure 1-4). The region of the sheet away from the clamped-ends show wrinkles under stretch. To study this problem, we follow a numerical approach using finite element method (FEM) with the ABAQUS code. Figure 1-5 schematically shows the boundary conditions in the uniaxial stress, uniaxial strain and clamped-ends stretching cases respectively.

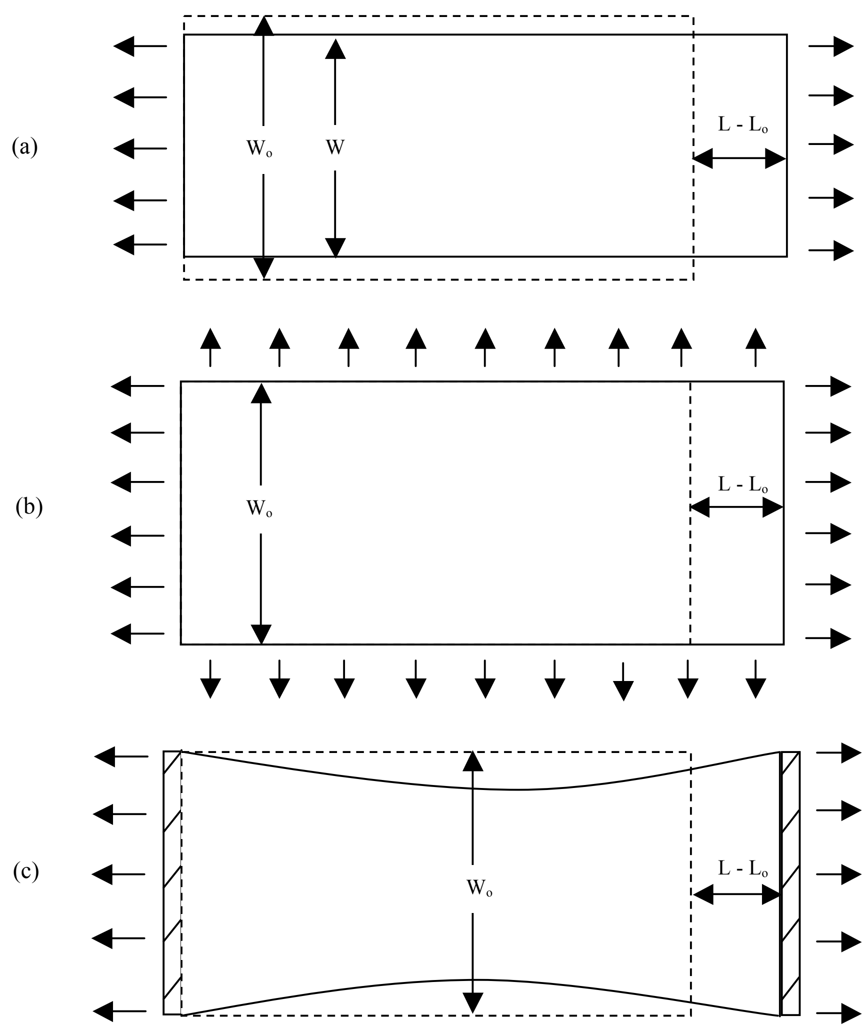

Figure 1-5: Schematic illustration of thin sheets under tension, (a) Uniaxial stress, (b) Uniaxial strain, (c) Clamped-ends stretching.

The boundary conditions in the present problem are neither of uniaxial stress case nor of uniaxial strain case. The boundary conditions here form a case in-between the two cases, therefore the force–strain plot for this case is expected to lie in between the uniaxial stress and uniaxial strain case. The analytical results for uniaxial stress and uniaxial strain case are presented in the next section.

1.4 Uniaxial stress in thin sheets

a) Small deformation

Uniaxial stress with small deformation can be assumed to have both geometrical and material linearity. The expression for force required to stretch the sheet is,

$$F = \sigma_1^n A_o = E A_o \varepsilon_x \tag{1.1}$$

where E is the Young's modulus of the material, ε_x is the nominal strain, $A_o = W_o t_o$ is the cross-section area and L_o ,W_o ,t_o is the length, width and thickness respectively of the sheet in original configuration.

b) Large deformation

In case of large deformation, both geometrical non-linearity and the material non-linearity shall be considered. For material non-linearity, Neo-Hookean hyperelastic model is used. Following relation is obtained assuming incompressible and isotropic material,

$$F = \sigma_1^n A_o = \mu A_o = \lambda_1 - \frac{1}{\lambda_1^2} \tag{1.2}$$

1.5 Uniaxial strain in thin sheets

a) Small deformation

Like the uniaxial stress case, the uniaxial strain problem is also discussed for small and large deformations. In this case, the relation for the small deformation with incompressibility is given as,

$$F = \frac{EA_o}{1-\nu^2}\varepsilon_x = \frac{4}{3}EA_o\varepsilon_x \tag{1.3}$$

b) Large deformation

The relation for the large deformation in uniaxial strain case can be written as,

$$F = \frac{\mu \mathrm{EA}_o}{3}\left(\lambda_1 - \frac{1}{\lambda_1^3}\right) \tag{1.4}$$

Figure 1-6 shows the analytical results for uniaxial stress and uniaxial strain together. It is noticeable that non-linearity in each case makes the structural behavior less stiff at high strains. Although the force required is almost same for linear and non-linear deformation at low strains, while there is a large difference between two at high strains. Therefore non-linearity must be considered in case of high strains. Also, the uniaxial strain case requires more force than uniaxial stress case because of the constraint on horizontal edges that does not allow them to shrink in the transverse direction. The clamped-ends stretching case as shown schematically in figure 1-5c lie in between these two cases, as also shown numerically in the following discussion.

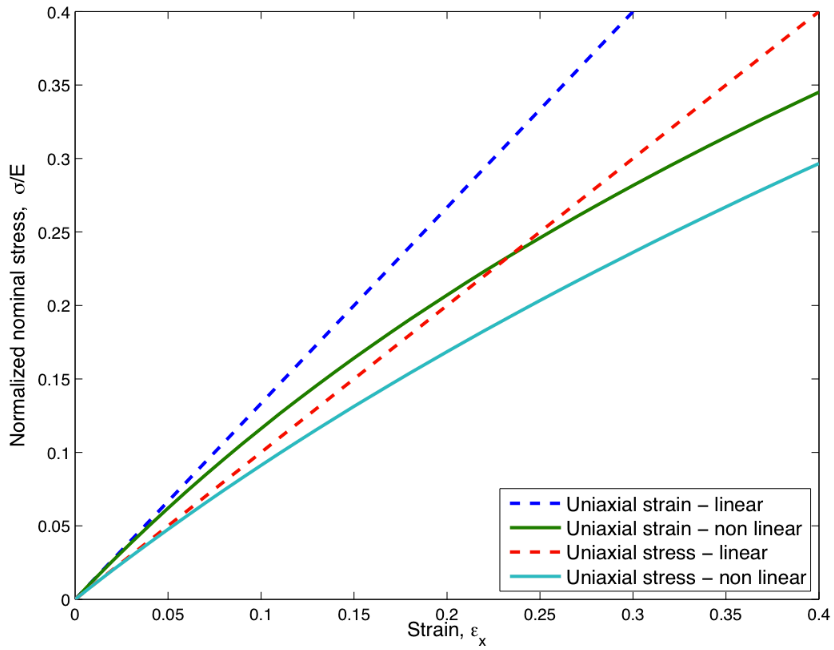

Figure 1-6: Comparison of analytical results for small and large deformation under uniaxial stress and uniaxial strain conditions.

1.6 Clamped-ends stretching of thin sheets

A plane stress finite element model (CPS4R) is used for the clamped-ends stretching case. The model problem is compared with the uniaxial stress and the uniaxial strain case considering small and large deformations. Figures 1-7 and 1-8 show that force-strain relation for the model problem lies in between the two cases. Figure 1-7 shows the linear deformation case whereas Figure 1-8 shows the non-linear deformation case. The uniaxial stress and strain cases form the lower and upper limits respectively to the response of the clamped-ends specimen. For smaller aspect ratios, the results of the clamped-ends specimen approach the uniaxial strain case, while those for higher aspect ratios the results approach the uniaxial stress case.

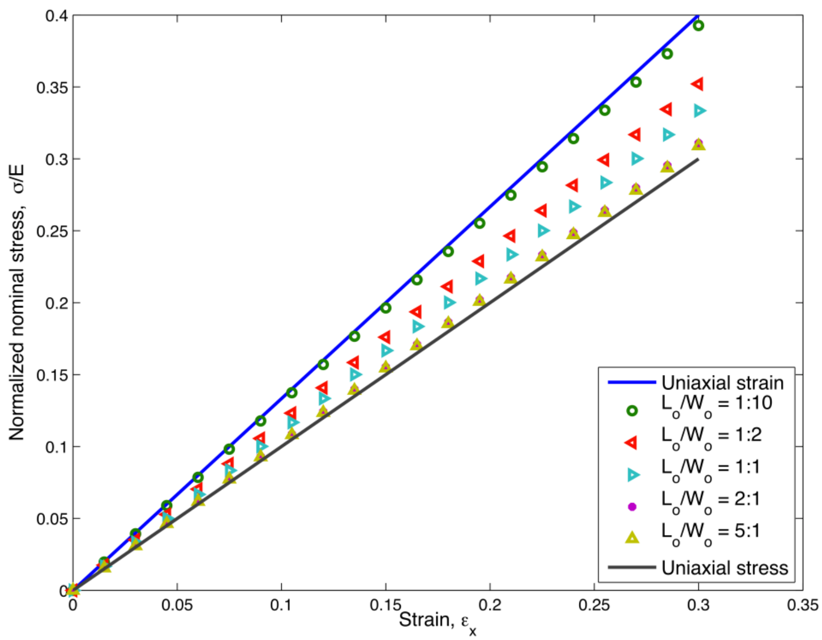

Figure 1-7: Comparison of force-strain results for clamped-ends stretching with different aspect ratios with uniaxial stress/strain case with linear geometry and linear elastic material.

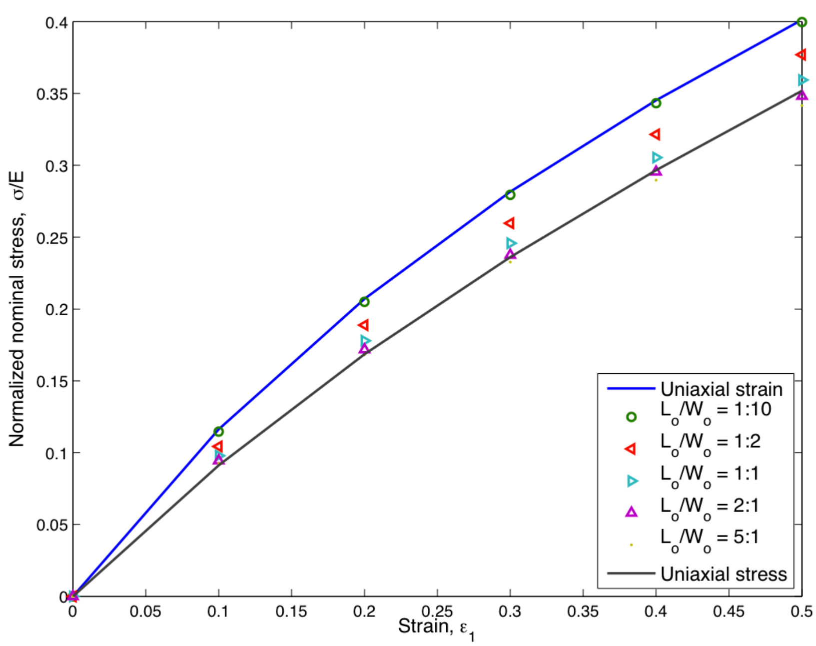

Figure 1-8: Comparison of force-strain results for clamped-ends stretching and uniaxial stress/strain case with non-linear geometry and non-linear elastic material.

1.7 Outline of thesis

The model problem has been discussed in this chapter. In Chapter 2, the stress state in the model problem will be discussed with emphasis on the development of compressive stress. Compressive stress is the most important aspect of this problem because it causes the wrinkles. We examine the effect of applied strain and aspect ratio on the compressive stress state. Since the deformation is highly non-linear, analysis incorporates non-linear geometry and elastic material properties.

In Chapter 3, eigen value buckling analysis is performed for the model problem. Analysis shows that buckling occurs only above a critical aspect ratio. Furthermore the perturbation analysis is done to check the instability of the modal problem. The instability in this case leads to wrinkling of the sheet. Prior to the perturbation analysis, number of modes to be used for applying imperfection and the effect of mesh size on the post-buckling analysis is also discussed.

In Chapter 4, the main results from the analysis and conclusions of the thesis are discussed.

2. Stretch-Induced Stresses in Thin Sheets

In Chapter 1 we discussed the model problem. In this chapter the stress analysis of the model problem is discussed. The primary interest here is to examine the compressive stress variation with the aspect ratio and the applied strain. A study of stresses in the thin sheets under clamped-ends stretching is shown in [15]; here we will discuss the variation in compressive stress state with aspect ratio and applied strain.

2.1 Stresses with clamped-ends stretching in linear elastic sheets

The stress analysis is performed using a plane stress-model (CPS4R) assuming that sheet remains flat during the entire course of loading. We begin with the discussion of different stress components in the clamped-ends stretching case. The material is considered to be linear elastic but geometric non-linearity is included.

Figure 2-1a shows a stress contour diagram of σ_x for $L_o/W_o = 1.5$ under 1% strain. Figure 2-1b shows the stress profile of σ_x along the path-1 as marked in figure 2-1a. Qualitatively the profile of the stress σ_x is similar at all strain levels and it is always tensile. It should be noted that σ_x does not have a large variation along the width of the sheet. Figure 2-1c shows the variation of stress σ_x at point A as a function of the applied strain. The stresses shown here are normalized by the Young's modulus to make the results independent of the material properties. The elastic boundary value problem indicates singularity at the corners of the sheet [16]; as seen in figure 2-1a, the finite element simulation does not resolve this singularity.

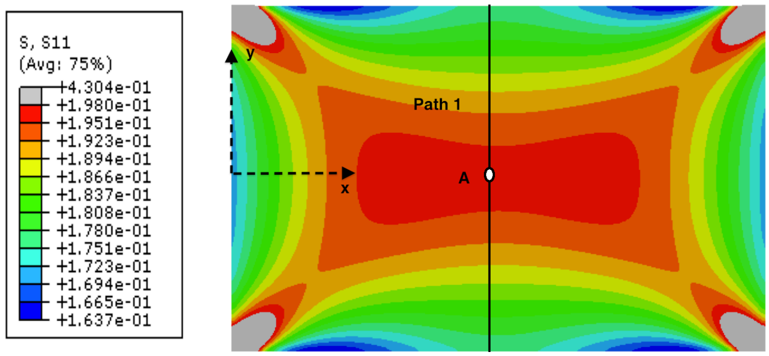

(a)

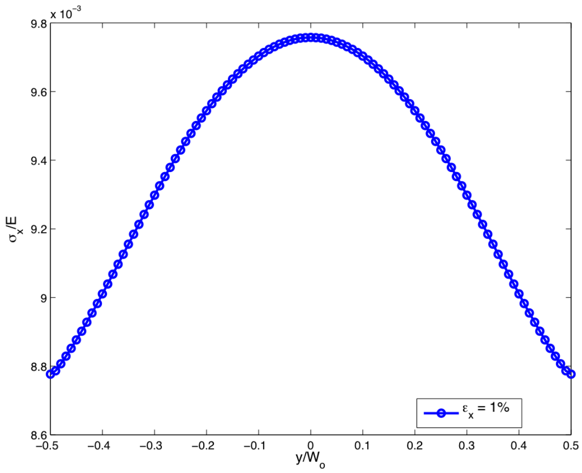

(b)

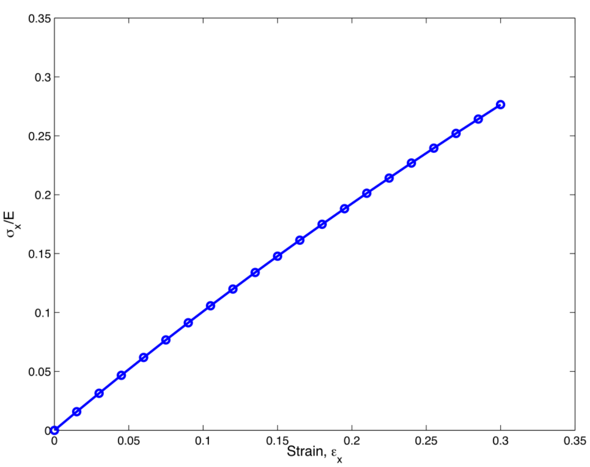

(c)

Figure 2-1: (a) Contour for σ_x at 1% strain for aspect ratio, L_o/W_o = 1.5, (b) Profile of σ_x along path-1 as marked in figure 2-1a at 1% strain for aspect ratio, L_o/W_o = 1.5, (c) Variation of σ_x with strain at point A as marked in figure 2-1a for aspect ratio, L_o/W_o = 1.5.

Figure 2-2a shows a stress contour diagram only of compressive part of σ_y for $L_o/W_o = 1.5$ under 1% strain. It should be noted that compressive stress is present only away from the clamped ends. Also, compression for the given modal problem is always observed in the transverse direction and σ_x is always positive in the sheet.

Figure 2-2b shows the stress profile for stress σ_y at 1% strain along path-1 as marked in figure 2-2a. As already mentioned that σ_y is negative with maximum compression occurring at the centre of the sheet for this aspect ratio. Unlike σ_x, stress profile for σ_y varies significantly depending upon both aspect ratio and applied strain applied. This variation of σ_y with aspect ratio and applied load will be discussed in the next section.

Figure 2-2c shows the variation of σ_y as a function of strain at point 'A'. It should be noted that stress σ_y at centre is not monotonically increasing as seen in case of σ_x. Stress σ_y reaches its peak value and then it starts to decay with increasing strain.

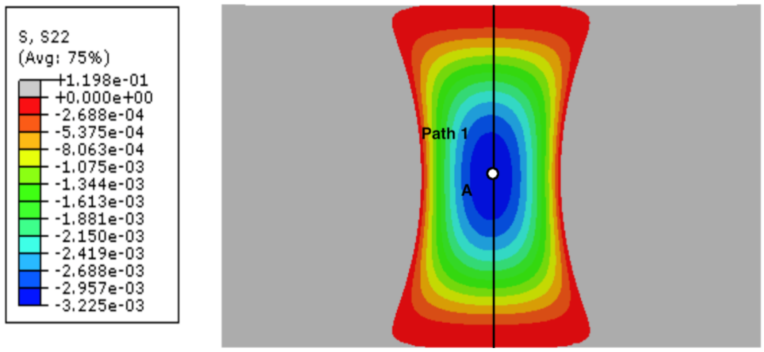

(a)

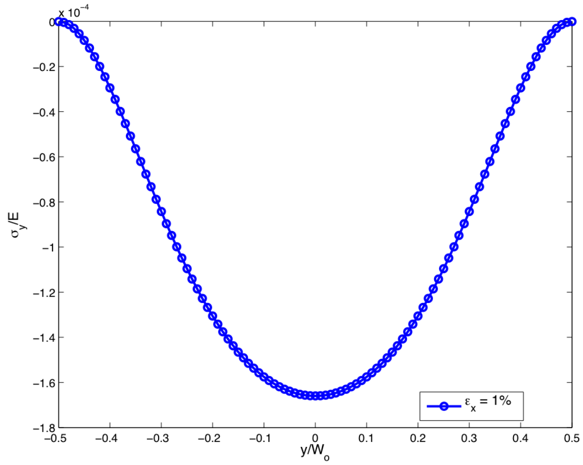

(b)

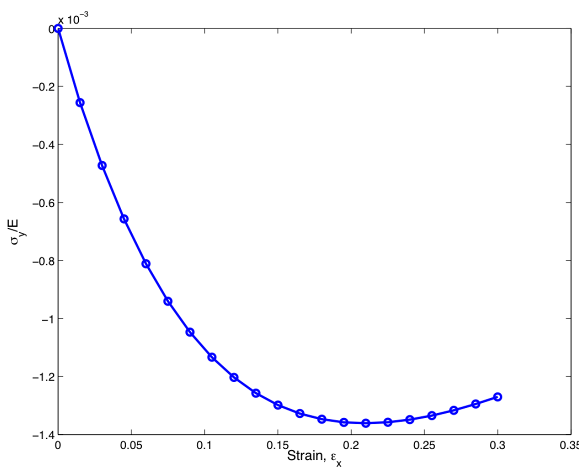

(c)

Figure 2-2: (a) Contour for σ_y (compressive) at 1% strain for aspect ratio, L_o/W_o = 1.5, (b) Profile of σ_y along path-1 as marked in figure 2-2a at 1% strain for aspect ratio, L_o/W_o = 1.5, (c) Variation of σ_y at point A as marked in figure 2-2a with applied strain for aspect ratio, L_o/W_o = 1.5.

Figure 2-3a shows a stress contour diagram of σ_{xy} for $L_o/W_o = 1.5$ under 1% strain. Figure 2-3b shows the stress σ_{xy} along paths 1 and 2 as marked in figure 2-3a at 1% strain. There is no shear at the centre (Path-1) but the clamped-ends of the sheet produces a shear stress (Path-2) due to the restraint at the edge. It should be noted that shear stress also exhibits a singularity at the corner due to the nature of the boundary conditions.

(a) 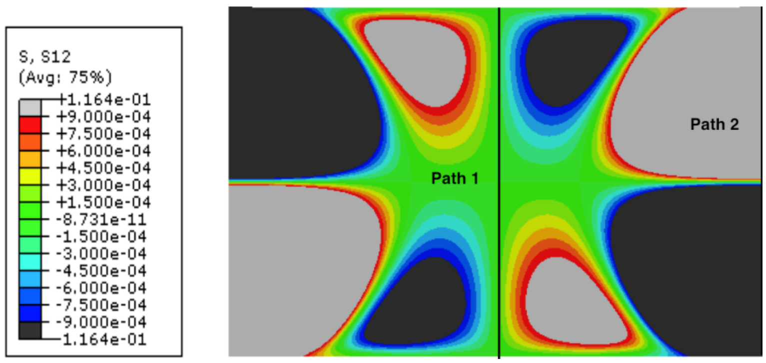

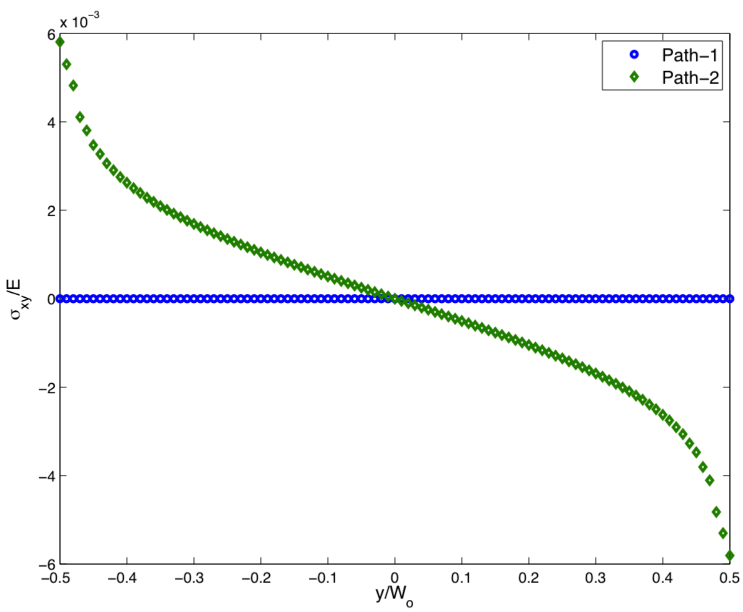

(b)

Figure 2-3: (a) Contour for σ_{xy} at 1% strain for aspect ratio, $L_o/W_o = 1.5$, (b) Profile of σ_{xy} along paths 1 and 2 as marked in figure 2-3a at 1% strain for aspect ratio, $L_o/W_o = 1.5$.

2.2 Distribution of σ_y in different aspect ratios with clamped-ends stretching for thin hyperelastic sheets

The distribution of different stress components is shown for $L_o/W_o = 1.5$ in the previous section. From here on, focus will be on the compressive stress in thin sheets (σ_y) and its dependence on both L_o/W_o and applied strain, as it is the cause for the wrinkling in thin sheets. From the analysis of σ_y stress in thin sheets for different aspect ratios, it is observed that the stress distribution of compressive σ_y shown in figure 2-2 is not similar for all L_o/W_o and ε_x. In this section we will show the distribution of compressive σ_y in thin sheets for different aspect ratios and the effect of strain on each type of distribution. The different types of σ_y distribution are named as different phases. Note that each phase signifies stress distribution of σ_y at the very beginning of the stretch, since for a given aspect ratio it can be in different phases depending upon the applied strain.

It should be noted that the stresses shown for L_o/W_o=1.5 are with linear elastic properties. Analysis with the linear elastic material properties has the following drawbacks:

- It is not applicable beyond a few percent of strain.
- It cannot quantitatively predict large-deformation behavior.

Therefore the following results are for nonlinear elastic material. Qualitatively, results shown in Section 2.1 are similar to the nonlinear elastic case and stress components have similar characteristics for same aspect ratio. For hyperelastic material, a Neo-Hookean model with incompressibility is used. Next we discuss the different types of σ_y distributions under clamped-ends stretching.

a. Phase 1 ($L_o/W_o \leq 1$)

Phase 1 does not show any compressive stress under tension as shown in figure 2-4a, showing the contour diagram for σ_y for a sheet with aspect ratio, $L_o/W_o = 1$, at 1% strain. Figure 2-4b shows the plot for σ_y along the path marked in figure 2-4a at different strain levels. It should be noted that there is only tensile stress in the sheet along the transverse direction for this range of aspect ratios, which increases with further strain.

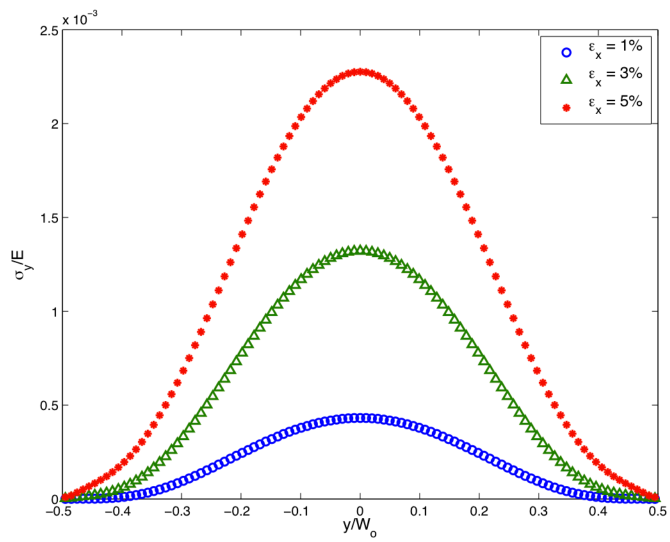

(a)

(b)

Figure 2-4: (a) Contour for σ_y in aspect ratio, $L_o/W_o = 1$ showing no compressive stress at 1% strain, (b) Distribution of σ_y along the path shown in figure 2-4a at different strain levels.

b. Phase 2 ($1 < L_o/W_o < 1.5$)

Phase 2 type of distribution is observed for $1 < L_o/W_o < 1.5$. For this range of aspect ratios, compressive stress is present in the transverse direction. In phase 2 the compression is concentrated in two regions along the transverse direction. Figure 2-5a shows only compressive σ_y in a sheet with aspect ratio, $L_o/W_o = 1.1$, at 1% strain. It should be noted that compressive stress is concentrated in two regions along y-direction. Figure 2-5b shows that the compressive σ_y initially reaches its peak and then it becomes zero with increasing strain. Same trend is observed in other phases also.

(a)
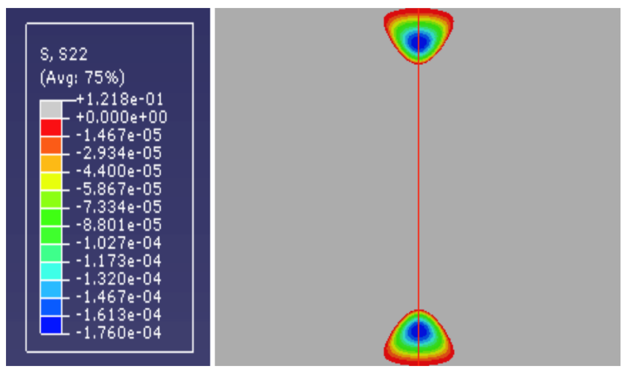

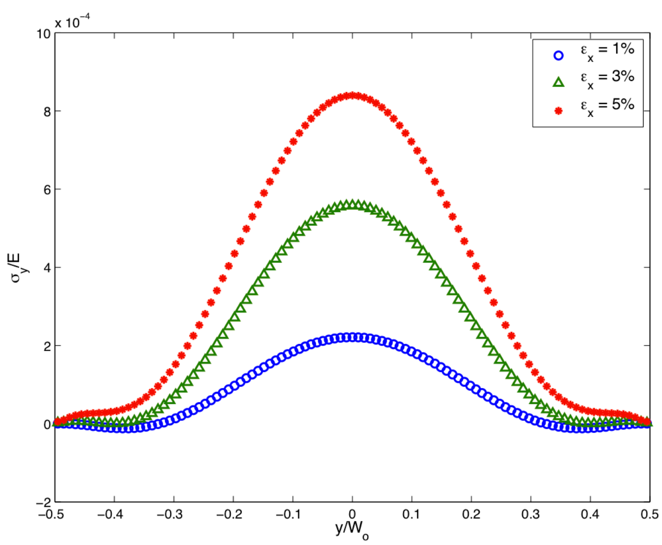

(b)

Figure 2-5: (a) Contour for σ_y in aspect ratio, $L_o/W_o = 1.1$ showing only compressive stress at 1% strain, (b) Distribution of σ_y along the path shown in figure 2-5a for aspect ratio, $L_o/W_o = 1.1$ at different strains

Figure 2-6a shows another example from phase 2. While for L_o/W_o=1.1, there is a tensile stress present between the two compressed regions, Figure 2-6a shows a stress contour for L_o/W_o=1.35, in which compression is present through out the width of the sheet. The compressive stress in the transverse direction still has two peaks as shown in figure 2-6b. Figures 2-6b shows an increase in the compressive stress with strain whereas Figure 2-6c shows decay in compressive stress with increasing strain. It should be noted that the compressive stress in the transverse direction disappears at about 15% strain. Hence with increasing strain the compressive stress distribution changes from phase 2 to phase 1. The critical strain required for this transformation depends upon the aspect ratio; for L_o/W_o =1.1 the critical strain observed is 3% whereas for L_o/W_o =1.35 it is 15%.

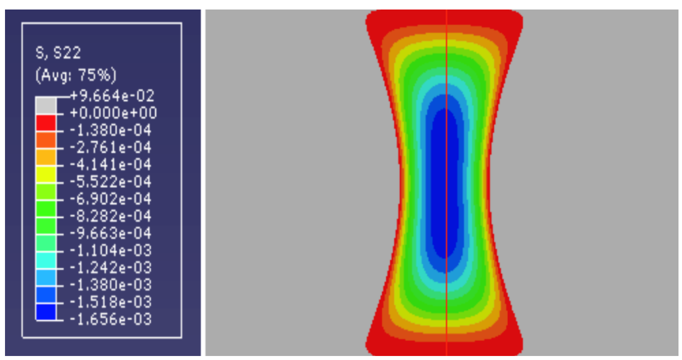

(a)

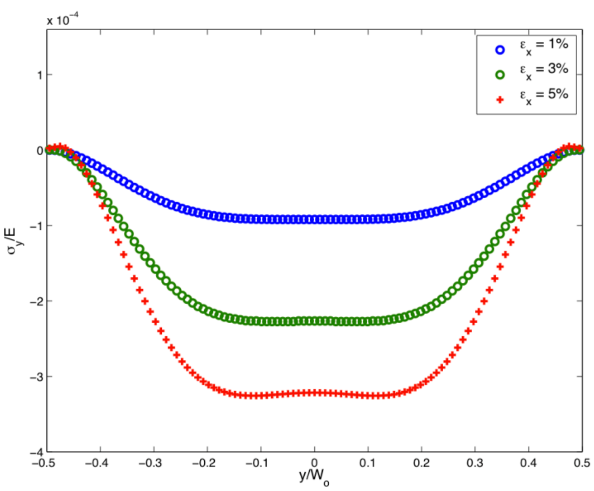

(b)

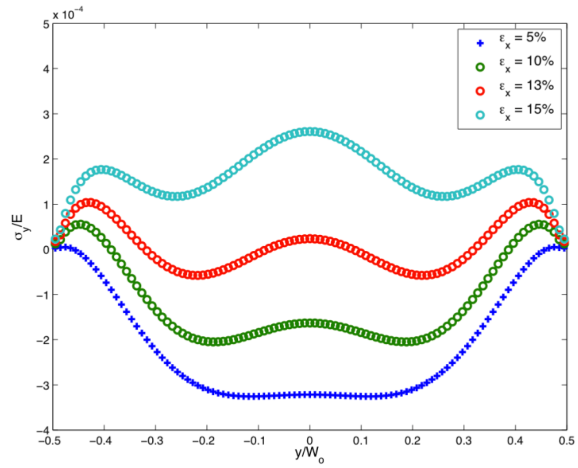

(c)

Figure 2-6: (a) Contour for σ_y in aspect ratio, $L_o/W_o = 1.35$ showing only compressive stress at 1% strain, (b) Showing increase in compressive stress with increasing strain, (c) Showing decrease in compressive stress with increasing strain.

c. Phase 3 ($1.5 \leq L_o/W_o < 2.2$)

In phase 3, compression is concentrated at the centre of the sheet. Figure 2-7a shows the contour diagram only for compressive σ_y for $L_o/W_o = 2$ at 1% strain. It can be seen from the stress profile of σ_y in figure 2-7b that the compression is concentrated at the centre. Figure 2-7b also shows the increase in compression with increase in strain until it reaches 20%. If strain is increased further, the compression starts to decay, as shown in Figure 2-7c. It should be noted that, at $\varepsilon_x = 60\%$, there is no compression in the sheet in the transverse direction. As already mentioned, for the transformation to take place, a critical strain, which is a function of aspect ratio, is required. Hence for this aspect ratio, the transformation takes place from phase 3 to phase 1 at 60% strain.

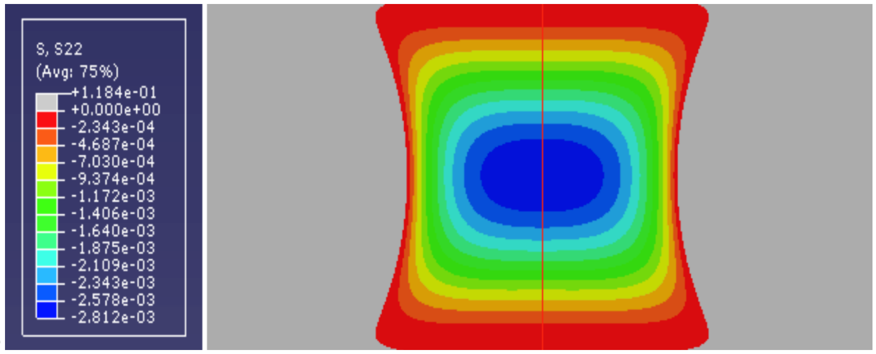

(a)

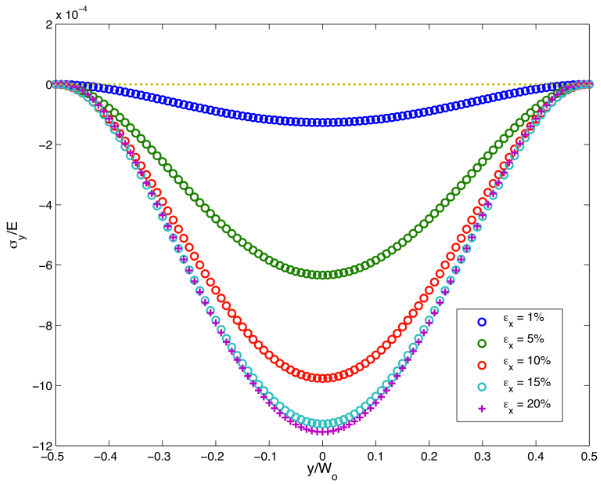

(b)

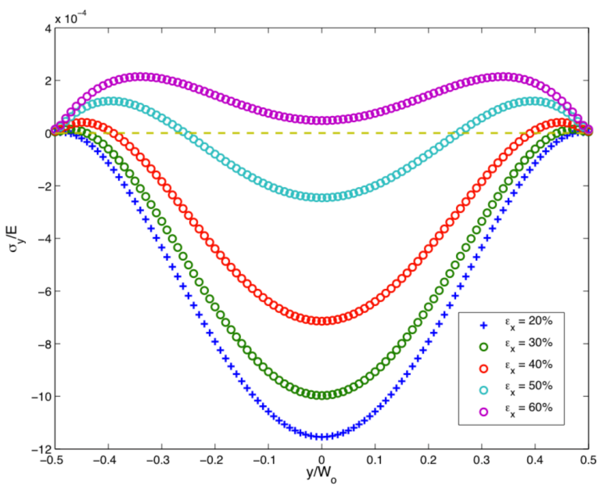

(c)

Figure 2-7: (a) Contour for σ_y in aspect ratio, $L_o/W_o = 2$ showing only compressive stress at 1% strain, (b) Showing increase in compressive stress with increasing strain, (c) Showing decrease in compressive stress with increasing strain.

d. Phase 4 ($2.2 \le L_o/W_o$)

In phase 3, compression was concentrated at the centre. When the aspect ratio is increased further the compressed region splits along the x-direction. This type of distribution of compressive stress with compression concentrated in two regions along the x-direction is referred to phase 4. Figure 2-8a shows the contour of compressive σ_y for $L_o/W_o = 2.5$ at 1% strain. The central region of the sheet is still under compression but now compression is concentrated in the two regions along the x-direction. Figure 2-8b shows the profile of σ_y along the x-direction. It also shows the increase in compressive stress with increasing strain (ε_x). Figure 2-8c shows that compressive stress start to decay if the strain is further increased above 20%.

The two peaks of compression present at the beginning, merge together as the strain is increased and at 60% strain, σ_y shows only one peak at the centre as shown in figure 2-8c. With further strain the compression can be removed completely. Hence in this case the transformation takes place from phase 4 to phase 3 and then to phase 1. This type of transformation takes place for $2.2 \le L_o/W_o < 4$.

Figure 2-9 shows the change in compressed region for $L_o/W_o = 2.5$ as the strain is increased. It should be noted that the region under compression becomes smaller with increasing strain and eventually it becomes compression free at a strain of 96% strain.

(a) 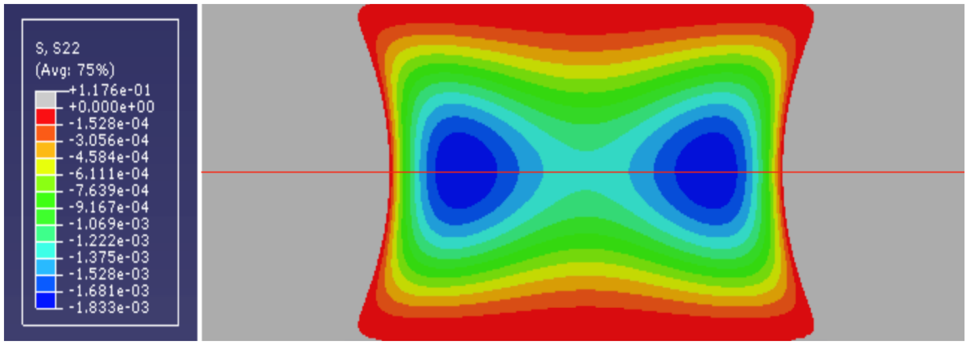

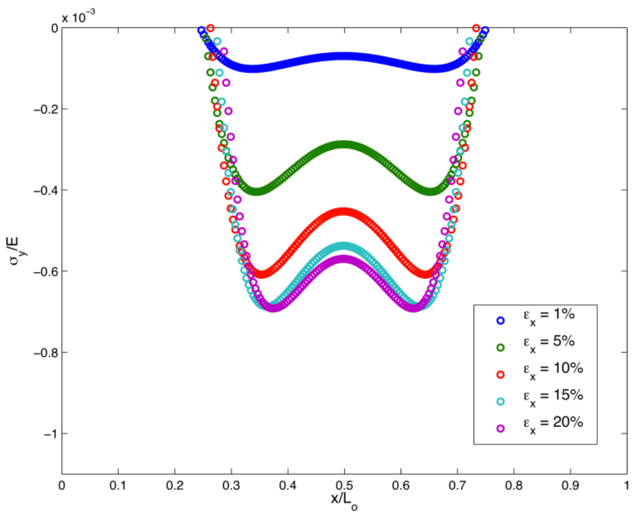

(b)

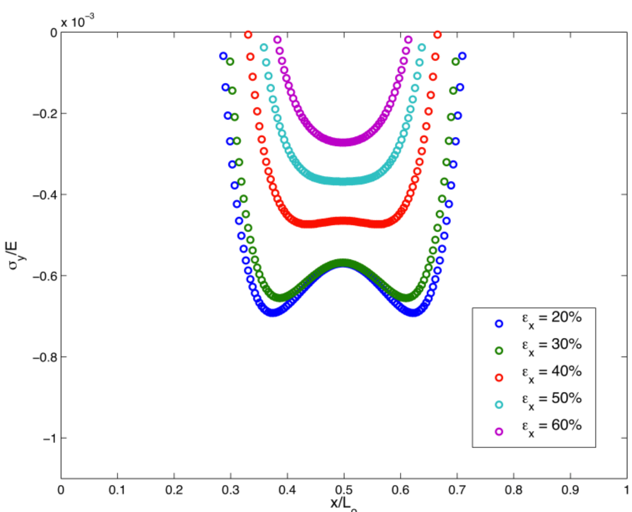

(c)

Figure 2-8: (a) Contour for σ_y in aspect ratio, $L_o/W_o = 2.5$ showing only compressive stress at 1% strain, (b) Showing increase in compressive stress with increasing strain, (c) Showing decrease in compressive stress with increasing strain.

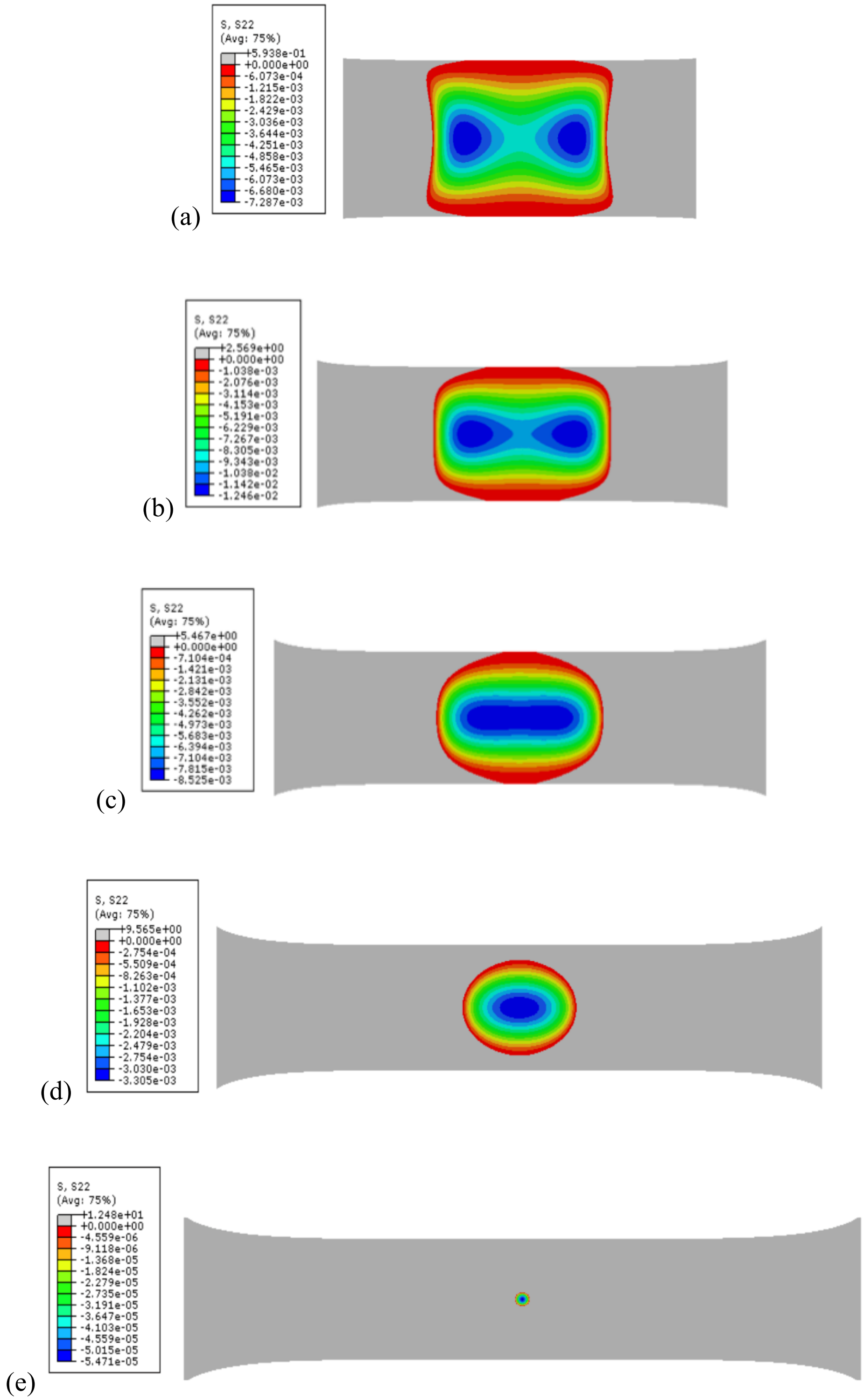

Figure 2-9: Showing the change in region under compression in a sheet with L_o/W_o = 2.5 under strain, (a) ε_x = 0.05, (b) ε_x = 0.2, (c) ε_x = 0.4, (d) ε_x = 0.75, (e) ε_x = 0.95

For longer aspect ratios, the sheet still exhibits phase 4 response. Figure 2-10a shows the stress contour of transverse compressive stress in a sheet with aspect ratio, $L_o/W_o= 5$, at 1% strain. It should be noted that the central region of the sheet has zero transverse stress. Under applied strain the compression occurs due to the clamped-ends boundary condition and the region of the sheet away from the clamped ends is not influenced by this boundary condition and hence it only shows uniaixal tension.

Figures 2-10b and 2-10c show the stress distribution along the path marked in figure 2-10a at different strain levels. Figure 2-10b shows increase in compressive stress as the strain is increased whereas Figure 2-10c shows the decay in compressive stress with further increase in strain. Unlike the previous case, two peaks of compression do no merge together with increasing strain and eventually the compression ends. For this reason, in all aspect ratios, $L_o/W_o > 4$, the phase transformation takes place directly from phase 4 to 1 under increasing strain. The critical strain at which the compression ends is shown for different aspect ratios in Figure 2-11. Next we will discuss the value of critical strain required for each aspect ratio to make it free of compression.

(a) 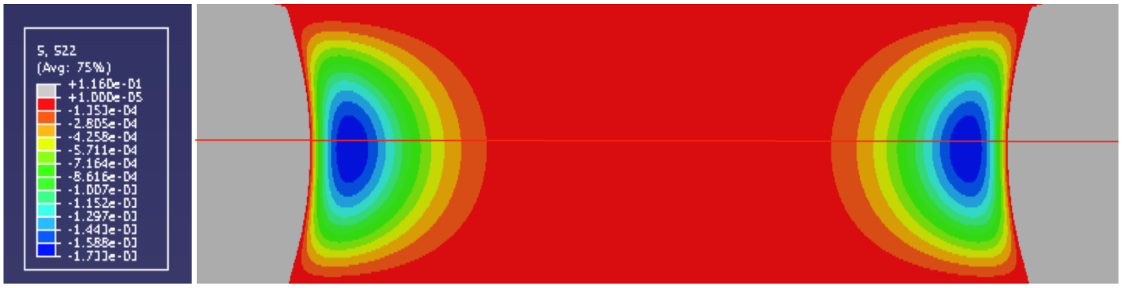

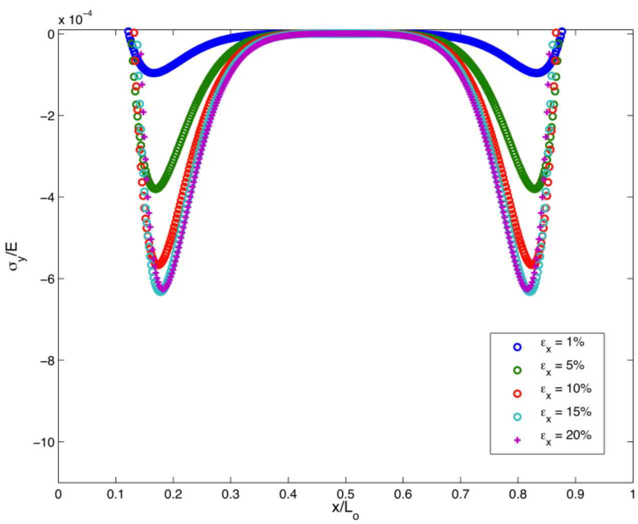

(b)

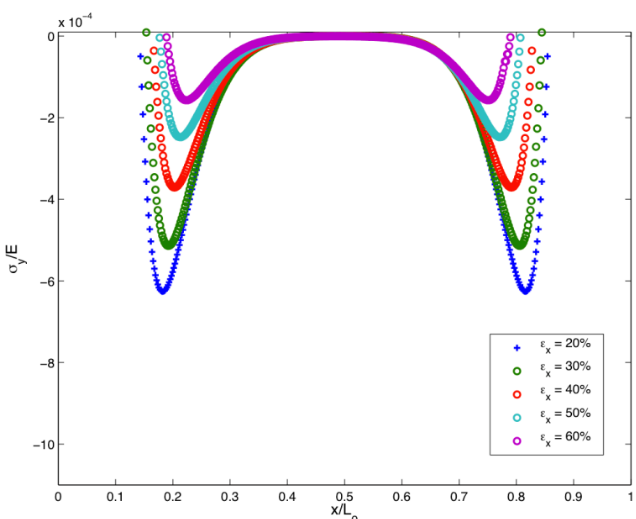

(c)

Figure 2-10: (a) Contour for σ_y in aspect ratio, $L_o/W_o = 5$ showing only compressive stress at 1% strain, (b) Showing increase in compressive stress with increasing strain, (c) Showing decrease in compressive stress with increasing strain.

2.3 Phase diagram

In the previous section, different phases of transverse compressive stress were shown. Dependence of compressive stress state on strain and aspect ratio was discussed and a critical strain at which phase 1 is achieved was also shown. Figure 2-11 summarizes this discussion; it shows the critical strain at which each aspect ratio changes to the compression free state (Phase 1) under clamped-ends stretching. The marked numbers refer to the phase shown by a sheet with a given aspect ratio and under applied strain. It also shows the different phases an aspect ratio undergoes before it finally changes to phase 1. It is observed from numerical calculations that the critical strain becomes almost constant for $L_o/W_o > 4$.

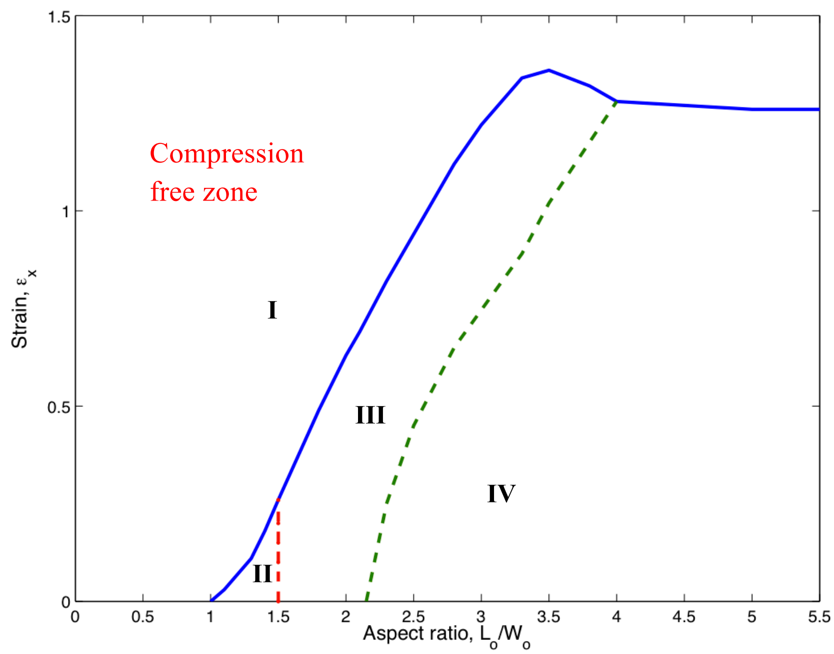

Figure 2-11: Showing critical strain for each aspect ratio above which there is no compression in hyperelastic thin sheets

Hence from this analysis with hyperelastic properties we can conclude that the compression occurring in the sheets is dependent on both strain and aspect ratio and for a given aspect ratio the compression can be removed by applying a required strain.

2.4 Comparison of σ_y for different aspect ratios

So far we have examined the compressive stress in the model problem for different aspect ratios separately. In this section we compare the stress σ_y in different aspect ratios with each other. The comparison is done for different aspect ratios at 1% strain. Figure 2-12 schematically shows the path along which the stress (σ_y) comparison is done. Here the stress profile is shown only for, $0 \leq x \leq L_o/2$ and $0 \leq y \leq W_o/2$, since the stresses are symmetrical about the centre.

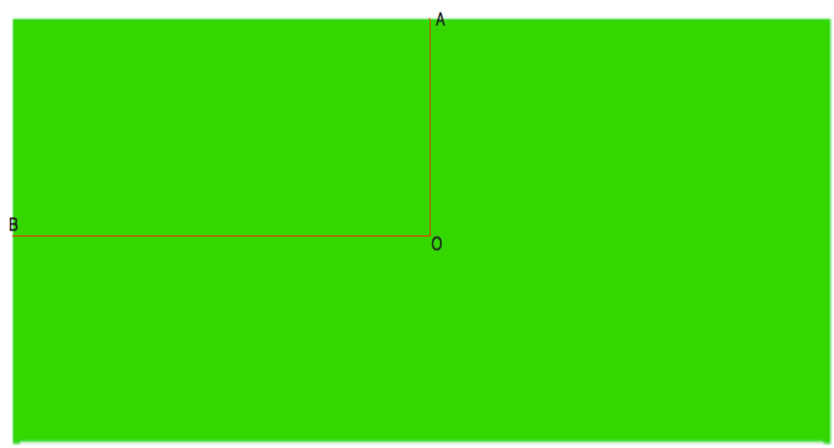

Figure 2-12: Showing the paths along which the stress σ_y is compared for different aspect ratios at 1% strain.

Figure 2-13 shows the stress σ_y along the path 'AO' as marked in figure 2-12. As already discussed in detail in Section 2.2, σ_y in a sheet depends on the aspect ratio. In the transverse direction, there is no compression for $L_o/W_o = 1$ (Phase 1), as seen in Figure 2-13. Further $L_o/W_o = 1.1$, belongs to phase 2 and it should have two peaks along transverse direction. Figure 2-13 shows only one of its region under compression, since the stress profile is shown only for halflength. For L_o/W_o = 1.5, which belongs to phase 3, σ_y has a single peak of compressive stress at the centre as clearly seen in figure 2-13. Next, aspect ratios, L_o/W_o = 2.5 and 5 belong to phase 4 which has two peaks of compression along x-direction. Along the transverse direction the stress in phase 4 may be compressive or zero depending upon the sheet length. If the aspect ratio is high (L_o/W_o > 4), the central region is free of transverse compressive stress, hence for L_o/W_o = 5, stress σ_y along 'AO' is zero whereas for lower range ($2.2 \leq L_o/W_o \leq 4$), the central region in-between the two maximum compression zones is also under the influence of compression, which is observed here for L_o/W_o = 2.5 in Figure 2-13.

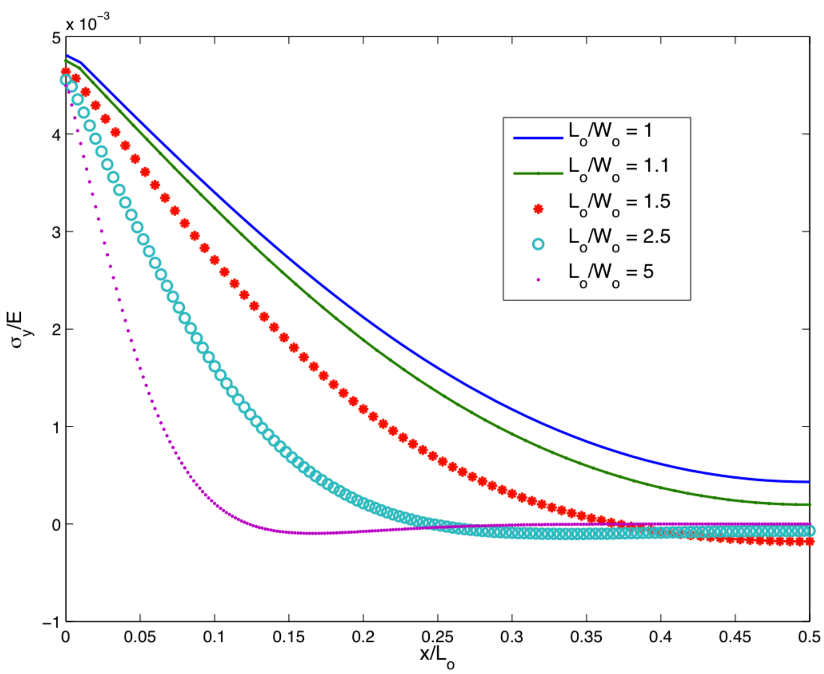

Figure 2-13: Showing stress σ_y in different aspect ratios at 1% strain along the distance 'AO' as marked in figure 2-12.

Figure 2-14 shows another comparison, for stress σ_y along the path 'BO' as marked in figure 2-12. For L_o/W_o = 1, there is no compression at all. For L_o/W_o = 1.1, compression is present near the free edges only as already discussed, hence figure 2-14 does not show any compression for this case. For L_o/W_o = 1.5, the compression is concentrated at the centre. For L_o/W_o = 2.5 and 5, σ_y has two peaks along x-direction which can be seen in figure 2-14. It should be noted that compression is always present away from the clamped-end boundary condition (x = 0) whereas in the previous comparison along y-direction, compression is present through out the width of the sheet with zero stresses at the free edges.

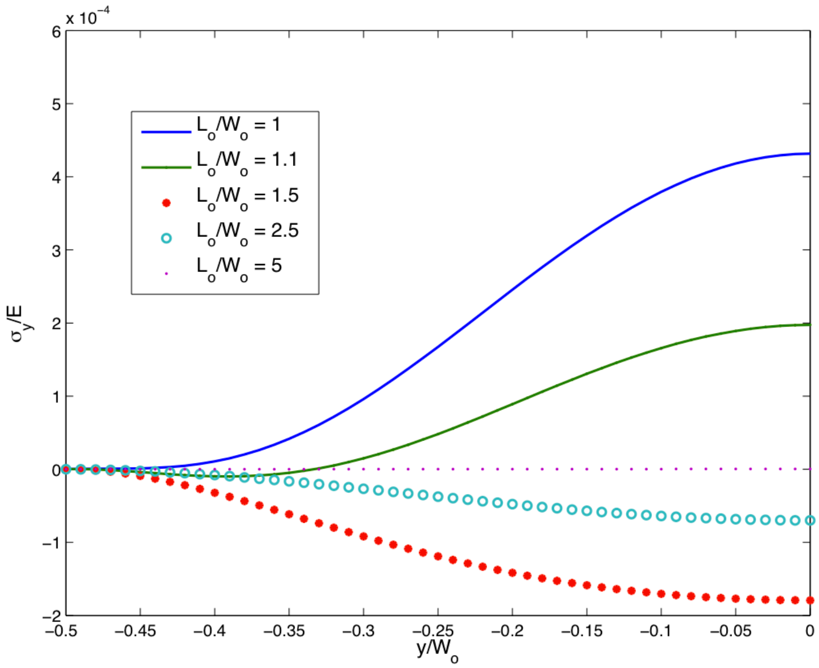

Figure 2-14: Showing stress σ_y in different aspect ratios at 1% strain along the distance 'BO' as marked in figure 2-12

Next we compare the variation of maximum compressive stress with strain. As shown in Section 2.2, the maximum compression can occur in different regions in a sheet depending upon the aspect ratio. Figure 2-15 shows maximum σ_y as a function of strain for different aspect ratios. It is observed that maximum compressive stress for any L_o/W_o increases with strain, reaches a maximum and then decreases. This maximum value increases with aspect ratio until $L_o/W_o \sim 2$ and then decreases, eventually saturating at about $L_o/W_o = 3$. Thus beyond aspect ratio, $L_o/W_o = 3$, the maximum compressive stress occurring in the sheet becomes almost constant. The strain at which the maximum compression occurs also saturates at about $L_o/W_o = 3$.

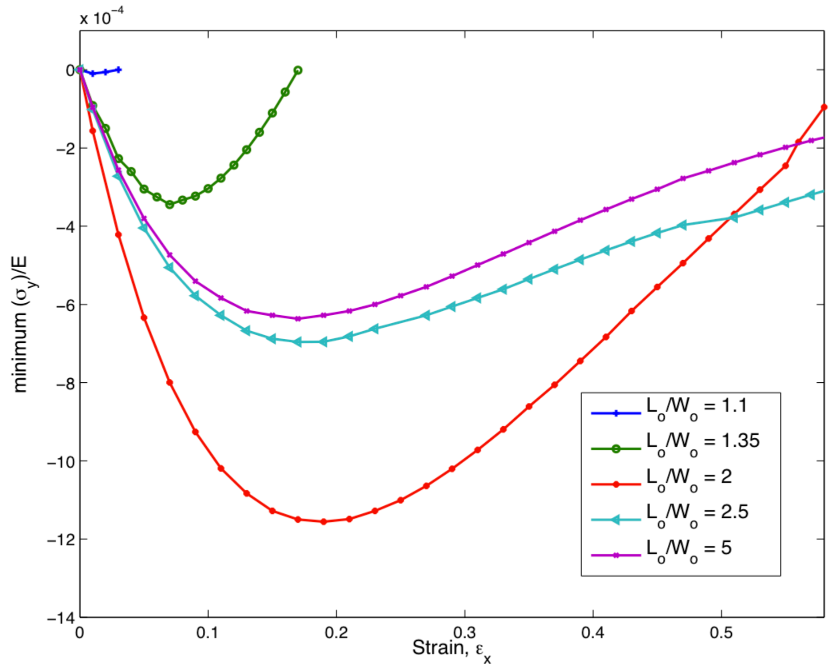

Figure 2-15: Showing the variation of maximum compressive stress with strain for different aspect ratios

This chapter gives us the idea of how the distribution of the compressive stress (σ_y) can vary with aspect ratio and applied strain. To apply high strains, hyperelastic material properties are used and it is noticed that as the strain is increased the transverse compressive stress becomes zero for any aspect ratio. The critical strain required for this transition to Phase 1 depends on the aspect ratio. In the next chapter we show the eigen value analysis to find the buckling modes for this problem and will see that buckling is related to compressive stress distribution and will also examine the behavior of wrinkles that form in thin sheets with different aspect ratios.

3. Stretch Induced Wrinkling in Thin sheets

In the previous chapter, the finite element results presented were obtained with a plane stress model. From here on, shell model will be used for the analysis of wrinkles. In this chapter we will show the eigen value analysis of the model problem to find the buckling modes under the given boundary conditions. Using the buckling modes a perturbation analysis is performed to examine the effect of stretch on a sheet with initial imperfection. The whole analysis is done for different aspect ratios, by varying the length of the sheet and keeping the width, W_o (= 10mm) and thickness, t_o (= 0.01mm) constant.

3.1 Eigen value analysis for clamped-ends stretching

For the buckling analysis, shell elements of type S4R with size '0.05 X 0.05' are used. The model has non-linear elastic (Neo-Hookean, incompressible) and non-linear geometric properties. In this analysis the Young's modulus is found to have no effect on the shape and size of wrinkles. In order to find the buckling modes of the sheet under stretch, the following sequence is used to perform the eigen value analysis. Initially a small strain ($\varepsilon_x \leq 1\%$) in the x-direction is applied to the sheet with clamped-ends boundary conditions. In the second step, the eigen value analysis is performed. The initial strain contributes in generating the compressive stress in the sheet and is necessary to find the buckling modes in this problem. Hence the eigen value analysis is done to seek the buckling modes, which are later used as perturbations in the post buckling analysis. From the eigen value analysis, it is observed that there is a lower limit of aspect ratio below which the buckling modes are not found for the model problem. This critical aspect ratio is found to be, L_o/W_o = 1.35. For higher aspect ratios the buckling modes are shown in the following section. The buckling modes obtained here can be related to the compressive σ_y distribution for different aspect ratios presented in the previous chapter. It should be noted from the following figures that buckling occurs only in the regions where compressive stress (σ_y) exists. Figure 3-1 show the 1st buckling mode under stretching for different aspect ratios. The buckling is observed after applying a pre-strain. The corresponding compressive stress distribution in a sheet under tension is shown in Section 2.2. It should be noted that the maximum out of plane deformation occurred only in the areas under compression. For instance, for L_o/W_o=1.35, the compressive stress has two peaks along transverse direction and the eigen value analysis also shows two regions of maximum deformation along the transverse direction.

(a)
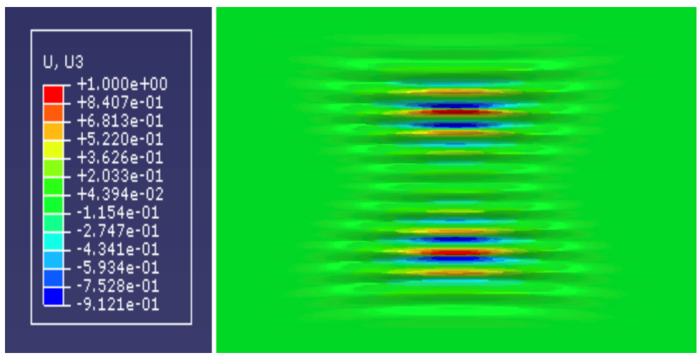

(b)
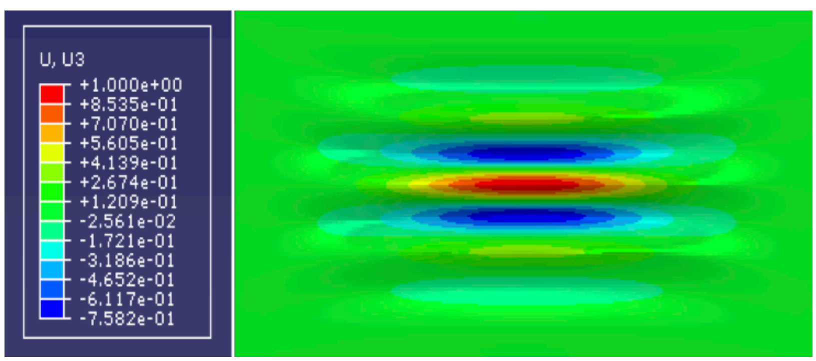

(c)
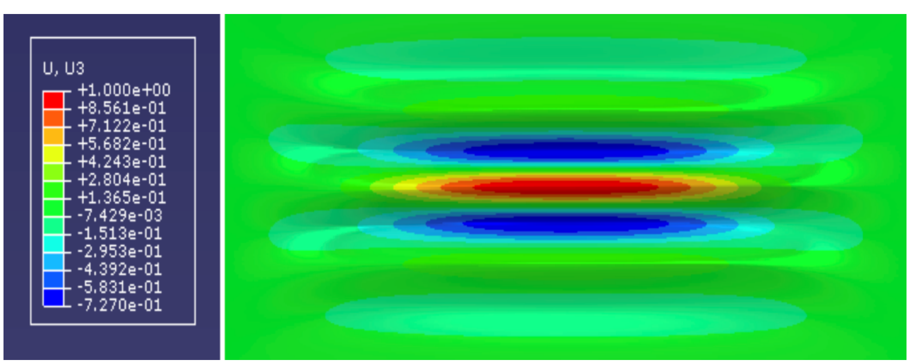

(d) 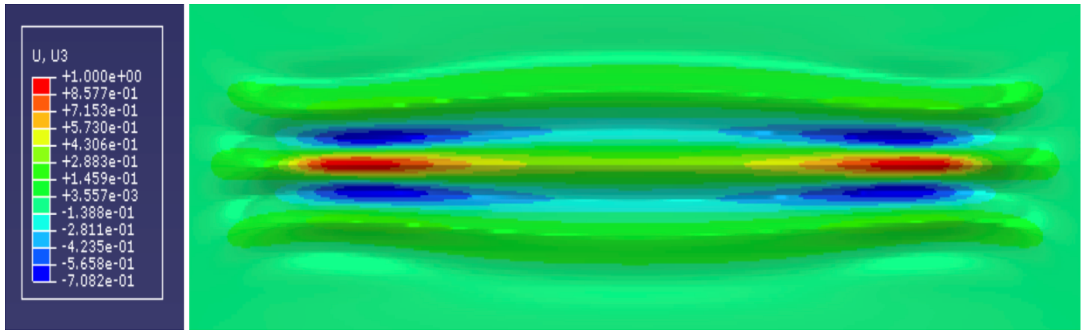

Figure 3-1: Showing 1st buckling mode occurring under clamped-ends stretching as obtained by eigen value buckling analysis for aspect ratio (a) L_o/W_o = 1.35, (b) L_o/W_o = 2, (c) L_o/W_o = 2.5, (d) L_o/W_o = 5.

3.2 Post-buckling analysis

For post-buckling analysis, a discussion of the number of buckling modes to be used for the initial imperfection is presented prior to the discussion of the wrinkle formation in different aspect ratios. The effect of mesh size and size of initial imperfection on the wrinkle formation is also discussed in the following section. To perform the perturbation analysis geometrical imperfections are applied using the eigen modes. The geometrical imperfections can also be applied using methods as explained in [17-18].

a) Effect of initial imperfection

First we will examine the effect of initial imperfection on the wrinkle analysis. It is found that the initial imperfection should be applied using 3 or more eigen modes to get a converged solution. It is also noticed that if only few buckling modes are used for perturbation, it shows different results with a slight change in the magnitude of initial imperfection. An example is shown through figure 3-2, which shows the post buckling results for L_o/W_o = 2.5, using only single buckling mode for initial imperfection with different imperfection sizes. Figure 3-2 shows a normalized plot of difference between maximum and minimum out-of-plane deformation vs the applied strain in the x-direction corresponding to the initial imperfection of 0.1% and 0.2% of thickness.

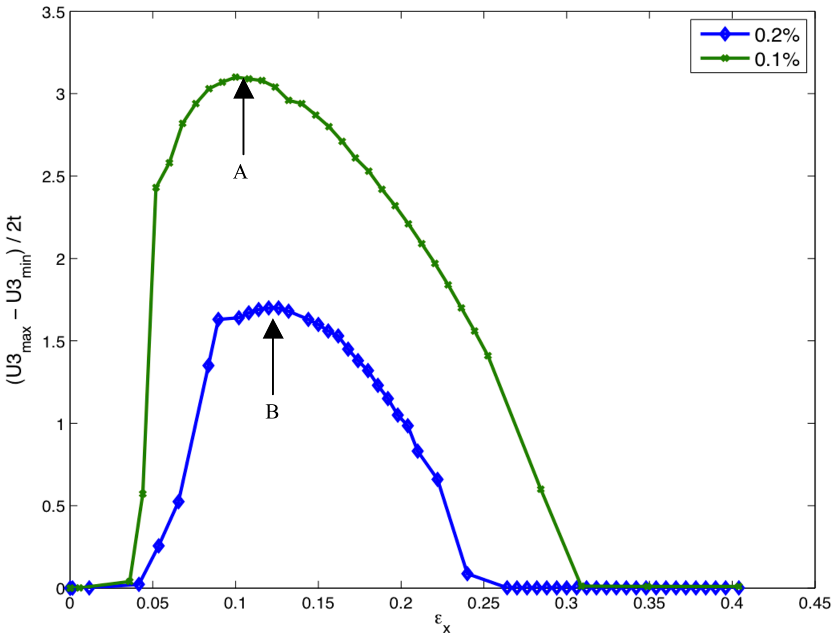

Figure 3-2: Results showing difference in wrinkle response with different size of initial imperfection by using only single buckling mode for initial imperfection.

This is also clearly seen through figures 3-3 and 3-4 where the form of wrinkles appearing in these two cases at their peak values (marked in figure 3-2 as 'A' and 'B') is shown. It can be seen that two cases exhibit significant differences. Note that the out-of-plane deformation magnitude shown here in figures 3-3 and 3-4 is the absolute deformation (mm) whereas Figure 3-2 shows the normalized deformation.

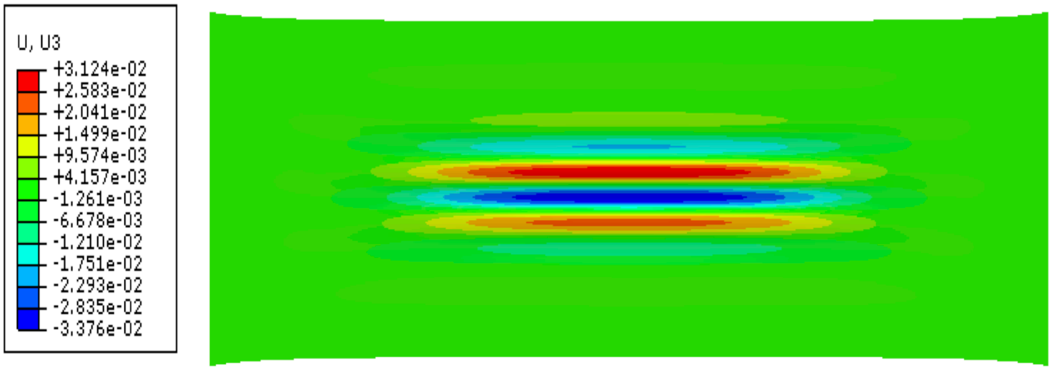

Figure 3-3: Shape of wrinkles formed with initial imperfection of 0.1% of thickness applied using only 1st buckling mode for imperfection. The aspect ratio is, $L_o/W_o = 2.5$ and the shape shown here corresponds to point 'A' as marked in figure 3-2.

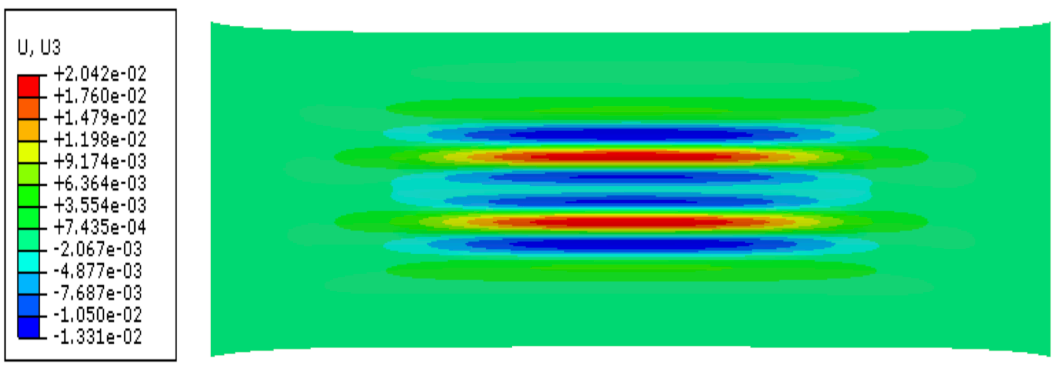

Figure 3-4: Shape of wrinkles formed with initial imperfection of 0.2% of thickness applied using only 1st buckling mode for imperfection. The aspect ratio is, $L_o/W_o = 2.5$ and the shape shown here corresponds to point 'B' as marked in figure 3-2.

Therefore, for the post buckling analysis, 5 buckling modes are used to represent the initial imperfection in performing wrinkle analysis. Figure 3-5 shows the wrinkle response with different initial imperfection size. It should be noted that by varying the imperfection size over a large range, the wrinkle response is very similar in each case. Hence it shows the convergence over the wrinkle response by using 5 eigen modes.

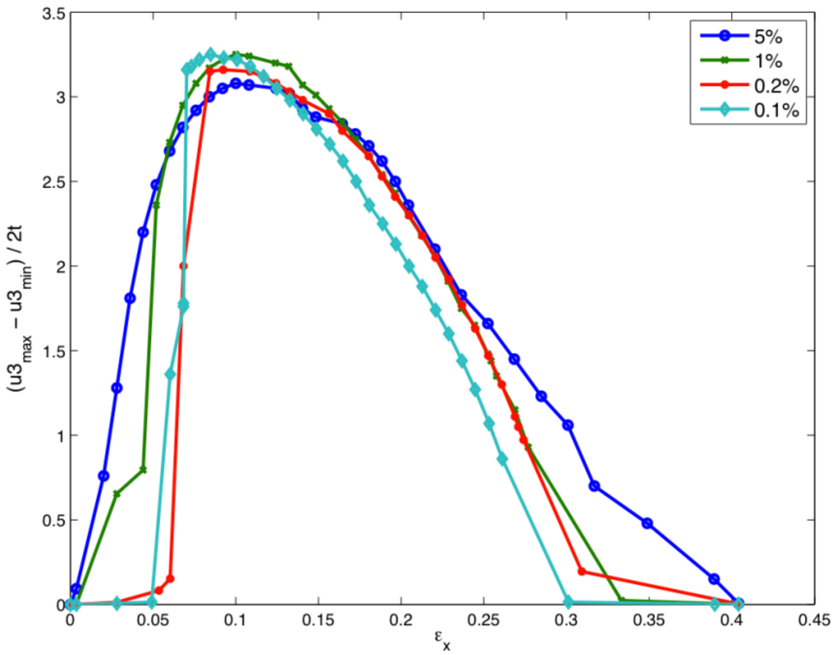

Figure 3-5: Results showing similar wrinkle behavior by using 5 buckling modes with different initial imperfection for aspect ratio, $L_o/W_o = 2.5$.

b) Effect of mesh size

The following analysis is done to investigate the effect of mesh size on the wrinkle formation. The aspect ratio used for this analysis is, $L_o/W_o = 2.5$. The results are shown in figure 3-6. The wrinkle amplitude is same in each case. Table 3-1 shows the size of elements in each of the mesh used for this analysis. The S4R type elements are used for this analysis with different sizes as mentioned in Table 3-1.

Table 3-1: Showing the size of elements in different meshes for $L_o/W_o = 2.5$

	Elements	Element size (mm X mm)
Mesh # 1	25000	0.1 X 0.1
Mesh # 2	39312	0.08 X 0.08
Mesh # 3	100000	0.05 X 0.05

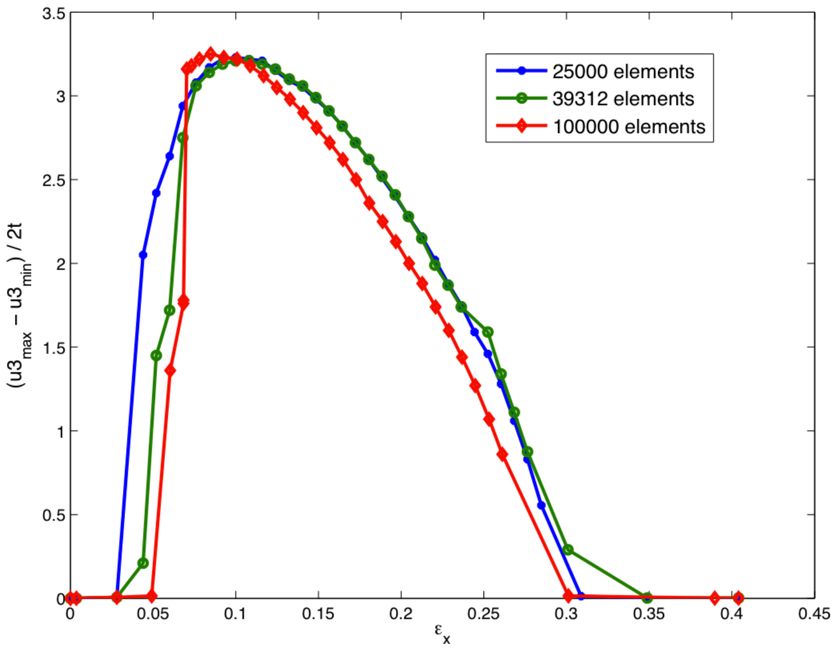

Figure 3-6: Showing the effect of mesh size on wrinkle formation for $L_o/W_o = 2.5$.

c) Wrinkle Formation

For the post-buckling analysis, 5 buckling modes with initial imperfection of 0.1% of thickness and mesh size of '0.05 X 0.05' is used for different aspect ratios. As already shown in Section 3-1, buckling occurs only in areas under compression. In the following section we discuss the post buckling analysis results for different aspect ratios. Buckling is not observed for aspect ratios lesser than, $L_o/W_o = 1.35$. For phase 1, no compression is seen under stretching, hence there is no buckling. For aspect ratios 1 to 1.35, the in-plane compressive stress is present but it is not sufficiently high to cause the buckling. For $L_o/W_o = 1.35$, although the eigen modes are seen but still the compressive stress (σ_y) is still not large enough and the out-of-plane deformation is very small as shown in figure 3-7.

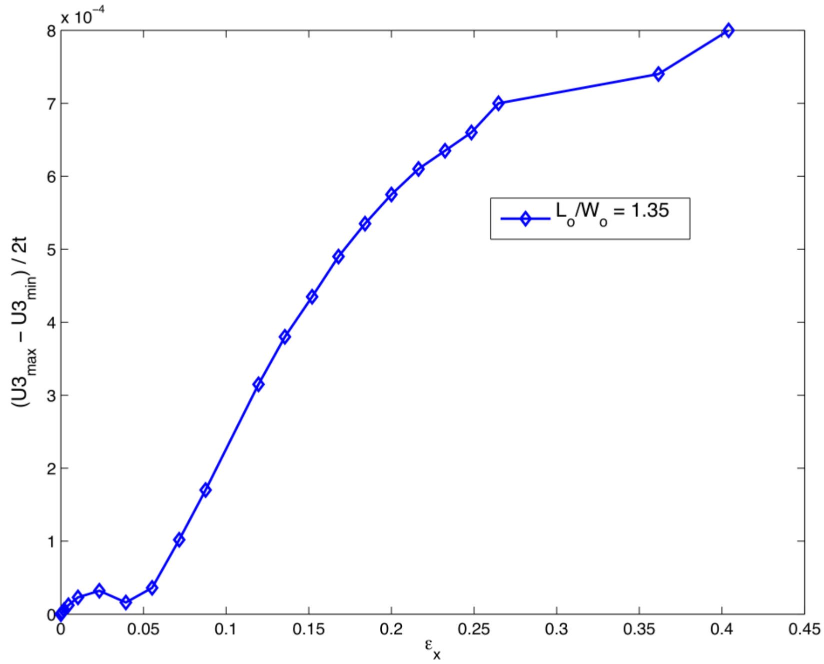

Figure 3-7: Showing wrinkle response with strain for aspect ratio, $L_o/W_o = 1.35$

For $L_o/W_o = 1.35$, σ_y has phase 2 distribution and it is the lowest aspect ratio for which buckling is observed. The small amplitude can be related to the low compressive stress observed in this aspect ratio. It should be noted that the wrinkle amplitude is still negligible, which is of the order of initial imperfection applied to sheet and there is not a significant instability observed in this case. There is only a slight growth from the initial imperfect state of the sheet.

For higher aspect ratios, the transverse compressive stress is higher and the out-of-plane deformation is also large. Figure 3-8 shows the wrinkle response of some of the higher aspect ratios. Maximum wrinkle amplitude is observed in $L_o/W_o = 2.5$. If aspect ratio is increased further, the wrinkle amplitude starts to decrease. In these cases the out-of-plane deformation occurs only for a range of strain and if the strain is lower or higher than that range, the sheet is unable to support the wrinkles. It should be noted that the out-of-plane deformation in this case is much larger than that shown in figure 3-7.

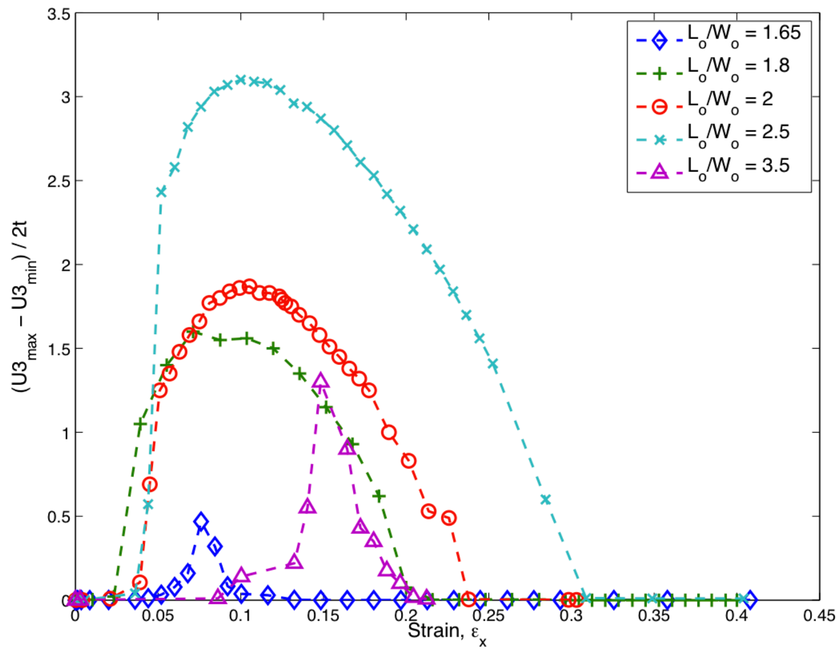

Figure 3-8: Wrinkle response with strain for different aspect ratios.

It can be noticed from Figure 3-8, in each aspect ratio the deformation is maximum at a certain strain level. Figure 3-9 shows that state of sheet at maximum out-of-plane deformation for different aspect ratios.

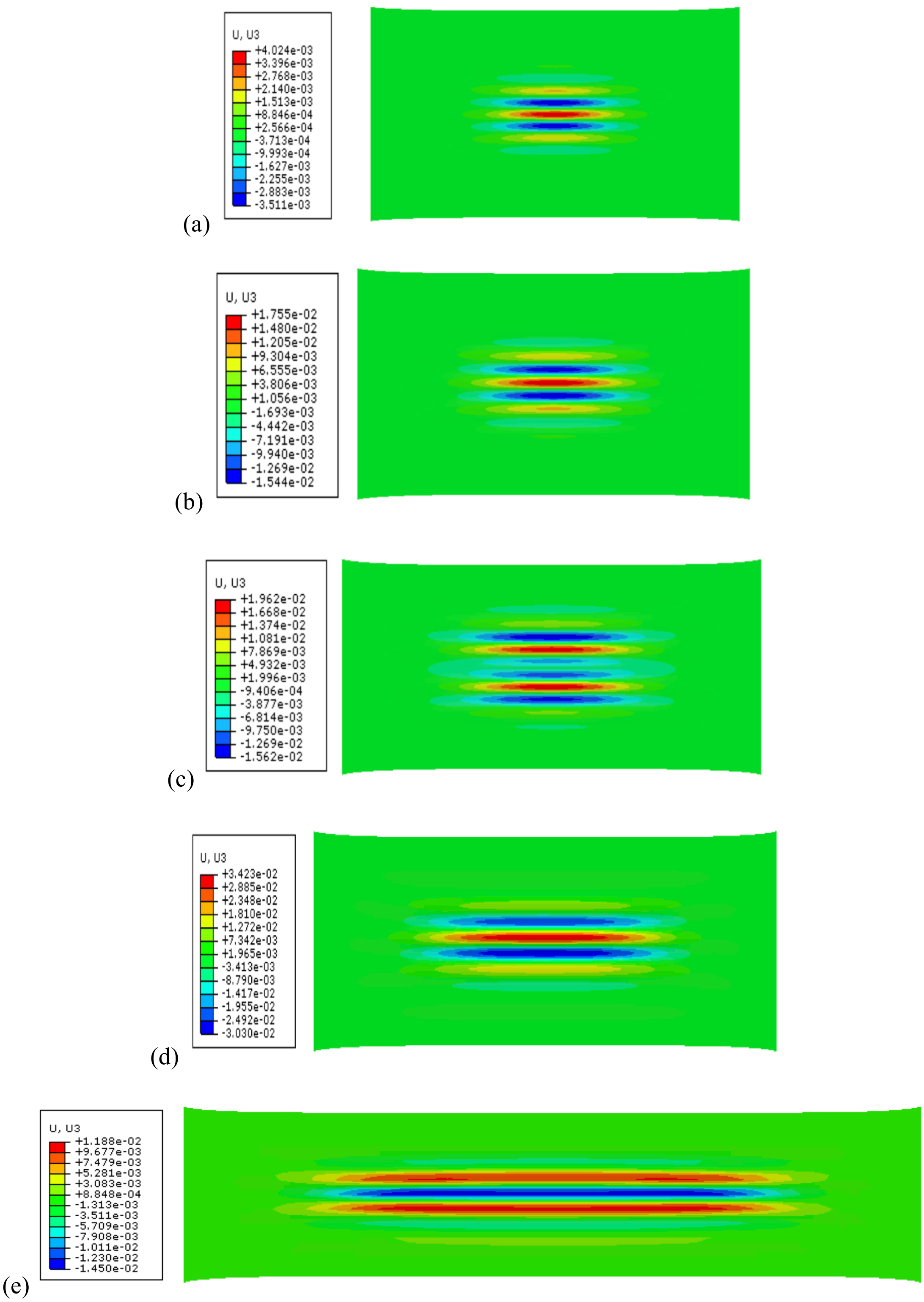

Figure 3-9: Showing wrinkle formation for aspect ratio, (a) $L_o/W_o = 1.65$, (b) $L_o/W_o = 1.8$, (c) $L_o/W_o = 2$, (d) $L_o/W_o = 2.5$, (e) $L_o/W_o = 5$ at their respective peak amplitude.

For different aspect ratios, the wrinkles start to form after a critical strain and then as the strain is increased the sheet gets flatten beyond a particular strain value.

Figures 3-10a and 3-10b summarize the wrinkle formation in different aspect ratios. Figure 3-10a shows the critical strain values for different aspect ratios, at which the wrinkles start to form, it reaches its peak value and finally when the wrinkles become negligible. Corresponding to the strain at which peak amplitude occurs, Figure 3-10b shows the value of the peak amplitude in each aspect ratio.

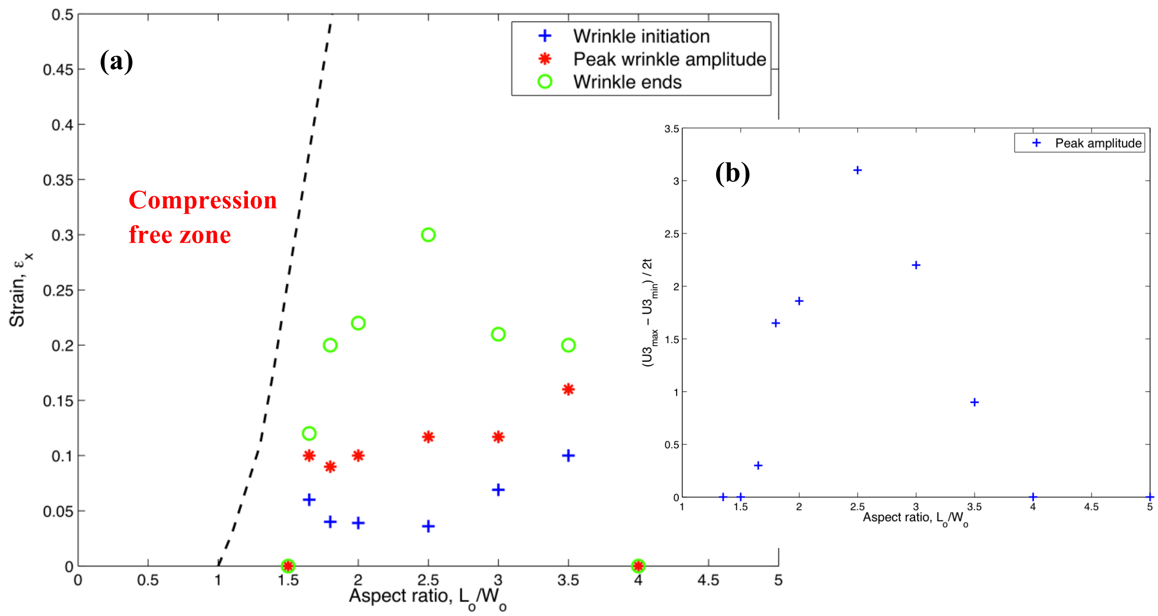

Figure 3-10: (a) Showing the critical strains at which wrinkle initiates, peaks and ends, (b) Showing the amplitude of the wrinkles when it peaks for the respective aspect ratios.

From Figure 3-10a it should be noted that for $L_o/W_o \leq 1.5$ and ≥ 4, the wrinkle formation is negligible. Figure 3-10a also shows a compression free zone as already shown in figure 2-11 also. In this zone no compression occurs whereas in the rest of the region, compression is present. Though compression is present in some range of L_o/W_o, it is observed that wrinkles form only for a specific range of applied strains for each aspect ratio. The range of strain for wrinkle formation will increase or decease according to the thickness of the sheet.

This analysis shows that the wrinkles are not permanent and the flatness of the sheet can be managed by the applied stretch. For these results, the sheet with elastic material properties is considered. Also, only some regions of compression are present in the sheets as it is stretched and the rest of the areas are not prone to wrinkles at all. It should be noted that this analysis is for a particular geometrical and material properties and if any of this gets changed, the range of strain in which the wrinkles form would be different.

4. Summary

In this chapter we will discuss the key findings of this thesis. The aim was to study the wrinkle formation in a thin sheet under clamped ends stretching. It is found that it is the compressive stress that occurs perpendicular to the direction of loading that leads to the buckling of the sheet and hence results in wrinkling. From the numerical analysis of the model problem we conclude that there are two main factors that affect the wrinkling and compression in the sheet, namely the aspect ratio and the applied strain, as discussed in the following section.

4.1 Effect of aspect ratio on stress and wrinkling

In this section we will summarize the effect of aspect ratio on the compressive stress distribution and buckling of sheets.

a) Effect of aspect ratio on stress

Apart from the numerical study of the compressive stresses as already shown in Chapter 2, there is another trend that is followed by the compression. It is how the regions under compression change as the sheet length is increased. Figures 2-4, 2-5, 2-6, 2-7, 2-8 and 2-9 show the variation in compressive stress from small to large aspect ratio. It is observed that for low aspect ratios, σ_y is always positive in the sheet under tension as shown in Figure 2-4. As the aspect ratio is increased, σ_y gets negative near the free edges of the sheet as shown in Figure 2-5. The compression starts from near the free edges and with increase in aspect ratio it spreads throughout the width of the sheet as shown in the Figure 2-6 with the compressive stress having two peaks along the transverse direction. Figure 2-7 shows the case for higher aspect ratio when the two peaks of compressive stress, σ_y along y-direction have merged together. Finally, for larger aspect ratios the compressed region splits along x-direction as shown in the Figures 2-8 and 2-9.

b) Effect of aspect ratio on wrinkling

The eigen value buckling analysis for the model problem shows that below an aspect ratio buckling is not possible. As shown in Section 3.1, for higher aspect ratios buckling occurs only with a pre-strain. The initial strain provides the compressive stress in the transverse direction to the sheet for buckling to occur for $L_o/W_o \geq 1.35$, whereas for aspect ratio, $L_o/W_o < 1.35$, no buckling is observed, because the compressive stress is insufficient.

4.2 Effect of strain on stress and wrinkling

a) Effect of strain on stress

The analysis shows that compressive stress start to decrease after a certain strain in each aspect ratio. For aspect ratios in which compression is present, it follows a common trend when strain is increased. As strain is increased the compressive stress reaches its maximum value and then starts to decay and eventually becomes zero. Hence there is a critical strain for each aspect ratio beyond which there is no compression in the sheet as shown in the figure 2-11.

b) Effect of strain on wrinkling

As already mentioned, the compressive stress reaches its peak value with applied strain and then it starts to decay. The wrinkles are related with certain stress level, so they form over a range of strain in which the compressive stress has the potential to cause wrinkles. If the stress is out of this range the wrinkles diminish in amplitude and the sheet regains its flatness.

This study also shows that the wrinkle prone regions depend upon the compressive stress distribution as shown in Section 3.1. The maximum out of plane deformation appears in the regions where the maximum compression occurs. Therefore by knowing the compressive stress distribution in the sheets, the areas where wrinkles can occur can be estimated.

Bibliography

[1] C. Talley, W. Clayton, P. Gierow, J. McGee and J. Moore. Advanced membrane materials for improved solar sail capabilities. In: Proc. 43rd AIAA/ASME/ASCE/AHS/ASC Structures, Structural Dynamics and Materials Conference, Denver, Colorado. AIAA 2002-1561 (2002).

[2] David W. Sleight, Yuki Michii, Troy O. Mann, Kara N. Slade and John T. Wang. Finite element analysis and test correlation of a 10-meter inflation-deployed solar sail. In: Proc. 46th AIAA/ASME/ASCE/AHS/ASC Structures, Structural Dynamics and Materials Conference, Austin, Texas. AIAA 2005-2121 (2005).

[3] Frederick H. Redell, Justin Kleber, David Lichodziejewski and GyulaGreschik. Inflatable-Rigidizable Solar Concentrators for Space Power Applications. In: Proc. 46th AIAA/ASME/ASCE/AHS/ASC Structures, Structural Dynamics and Materials Conference, Austin, Texas.AIAA 2005-1879 (2005).

[4] V. Peypoudat, B.Defoort, D. Lancour, P. Brassier, O. Le Couls, S. Langlois, S. Lienard, M. Bernasconi, M. Gotz. Development of a 3.2m-long inflatable and rigidizable solar array breadboard. In: Proc. 46th AIAA/ASME/ASCE/AHS/ASC Structures, Structural Dynamics and Materials Conference, Austin, Texas.AIAA 2005-1881 (2005).

[5] Hiraku Sakamoto and K.C. Park. Design parameters for wrinkle reduction in membrane space structures. In: Proc. 46th AIAA/ASME/ASCE/AHS/ASC Structures, Structural Dynamics and Materials Conference, Austin, Texas.AIAA 2005-1974 (2005).

[6] Pellegrino, S., Green, C., Guest, S. D., and Watt, A. SAR advanced deployable structure. Tech. Rep. CUED/D-STRUCT/TR191, University of Cambridge, Department of Engineering, Cambridge, UK (2000).

[7] http://www.ilcdover.com/products_ad_se_inflatable_antennas.cfm.

[8] http://www.nasa.gov/centers/marshall/multimedia/photos/2005/photos05-039.html.

[9] Wong, Y.W., and Pellegrino, S. Wrinkled membranes. Part I: experiments. Journal of Mechanics of Materials and Structures, 1(1), 1-23 (2006).

[10] Wong, Y.W., and Pellegrino, S. Wrinkled membranes. Part II: analytical models. Journal of Mechanics of Materials and Structures, 1(1), 25-59 (2006).

[11] Wong, Y.W., and Pellegrino, S. Wrinkled membranes. Part III: numerical simulations. Journal of Mechanics of Materials and Structures, 1(1), 61-93 (2006).

[12] T. Iwasa, M.C. Natori, K. Higuchi. Evaluation of tension field theory for wrinkling analysis with respect to the post-buckling study. Journal of Applied Mechanics, 71, 532-540(2004).

[13] E. Cerda, K. Ravi-Chandar and L. Mahadevan. Wrinkling of an elastic sheet under tension. Nature, Vol.419, 579-580 (2002).

[14] E. Cerda and L. Mahadevan. Geometry and Physics of Wrinkling. Physical Review Letters, Vol.90, 074302 (2003).

[15] N. Friedl, F.G. Rammerstorfer, F.D. Fisher. Buckling of stretched strips. Computers and Structures, Vol.78, 185-190 (2000).

[16] J. Benthem, Q. J. Mech. Appl. Math. 16, 413 (1963).

[17] Leifer, J., and Belvin, W. K. Prediction of wrinkle amplitudes in thin film membranes using finite element modeling. 44th AIAA/ASME/ASCE/AHS/ASC Structures, Structural Dynamics and Materials Conference, Norfolk, VA. AIAA 2003-1983 (2003).

[18] Alexander Tessler, David W. Sleight, and John T. Wang. Effective Modeling and Nonlinear Shell Analysis of Thin Membranes Exhibiting Structural Wrinkling. Journal of Spacecraft and Rockets, Vol.42, No.2, 287-298 (2005).

[19] JohanMansson and Johan Soderqvist. Finite Element Analysis of Thin Membrane Wrinkling. MSc Thesis, Department of Mechanics, Royal Institute of Technology, Stockholm (2003).

[20] ABAQUS. Theory and User's Manual. Version 6.8 (2008).

[21] Su, Xiaofeng, and Frank, Abdi. Wrinkling analysis of a Kapton square membrane under tensile loading. In: Proc. 44th AIAA/ASME/ASCE/AHS/ASC Structures, Structural Dynamics and Materials Conference, Norfolk, VA.AIAA 2003-1985 (2003).

[22] Eung-Shik Lee and Sung-Lie Youn. Finite element analysis of wrinkling membranes structures with large deformations.Finite Elements in Analysis and Design 42, 780-791 (2006).

[23] Keejoo, Lee, and Lee, Sung W. Analysis of gossamer space structures using assumed strain formulation solid shell elements. In: Proc. 43rd AIAA/ASME/ASCE/AHS/ASC Structures, Structural Dynamics and Materials Conference, Denver, Colorado.AIAA 2002-1559 (2002).

[24] AdamaDiaby, Anh Le van and Christian Wielgosz. Buckling and wrinkling of prestressed membranes. Finite Elements in Analysis and Design 42, 992-1001 (2006).

[25] Xiaoyun Wang, Wanping Zheng and Yan-Ru Hu. Active Flatness Control of Membrane Structures Using Adaptive Genetic Algorithm. In: Proc. SPIE, Industrial and Commercial Applications of Smart Structures Technologies, San Diego, CA. Vol. 6572, 652704 (2007).

VITA

Vishal Nayyar was born in Amritsar, India. After completing his work at Bhavan's SL Public School he moved to DAV College Amritsar. In 2004 he got admitted to Panjab University, Chandigarh, India. Here he completed his Bachelor Degree in Mechanical Engineering with Honours in 2008. In August he entered the Graduate School at The University of Texas at Austin.

Email address:	vishal.uta@gmail.com
Permanent Address:	68-C, Krishna Square 2
	Shivala Road, Amritsar-143001
	India

This thesis was typed by Vishal Nayyar.